AGU100 ADVANCING EARTH AND SPACE SCIENCE

Earth and Space Science

RESEARCH ARTICLE
10.1029/2018EA000408

**Special Section:**
Planetary Mapping: Methods, Tools for Scientific Analysis and Exploration

**Key Points:**
- Hasselblad surface photographs were registered to LROC NAC orthoimages
- Astronaut and instrument positions were determined by angular network adjustments
- A new Apollo 17 Traverse Map and large-scale station maps are provided

**Supporting Information:**
- Supporting Information S1
- Table S1

**Correspondence to:**
I. Haase,
isabel.haase@tu-berlin.de

**Citation:**
Haase, I., Wählisch, M., Gläser, P., Oberst, J., & Robinson, M. S. (2019). Coordinates and maps of the Apollo 17 landing site. *Earth and Space Science*, *6*, 59–95. https://doi.org/10.1029/2018EA000408

Received 30 APR 2018
Accepted 28 OCT 2018
Accepted article online 7 DEC 2018
Published online 12 JAN 2019



# Coordinates and Maps of the Apollo 17 Landing Site

**Isabel Haase[1], Marita Wählisch[2], Philipp Gläser[1], Jürgen Oberst[1,2], and Mark S. Robinson[3]**

[1]Department of Planetary Geodesy, Technical University Berlin, Berlin, Germany, [2]Department of Planetary Geodesy, German Aerospace Center (DLR), Berlin, Germany, [3]School of Earth and Space Exploration, Arizona State University, Tempe, AZ, USA

**Abstract** We carried out an extensive cartographic analysis of the Apollo 17 landing site and determined and mapped positions of the astronauts, their equipment, and lunar landmarks with accuracies of better than ±1 m in most cases. To determine coordinates in a lunar body-fixed coordinate frame, we applied least squares (2-D) network adjustments to angular measurements made in astronaut imagery (Hasselblad frames). The measured angular networks were accurately tied to lunar landmarks provided by a 0.5 m/pixel, controlled Lunar Reconnaissance Orbiter Camera (LROC) Narrow Angle Camera (NAC) orthomosaic of the entire Taurus-Littrow Valley. Furthermore, by applying triangulation on measurements made in Hasselblad frames providing stereo views, we were able to relate individual instruments of the Apollo Lunar Surface Experiment Package (ALSEP) to specific features captured in LROC imagery and, also, to determine coordinates of astronaut equipment or other surface features not captured in the orbital images, for example, the deployed geophones and Explosive Packages (EPs) of the Lunar Seismic Profiling Experiment (LSPE) or the Lunar Roving Vehicle (LRV) at major sampling stops. Our results were integrated into a new LROC NAC-based Apollo 17 Traverse Map and also used to generate a series of large-scale maps of all nine traverse stations and of the ALSEP area. In addition, we provide crater measurements, profiles of the navigated traverse paths, and improved ranges of the sources and receivers of the active seismic experiment LSPE.

**Plain Language Summary** We have identified the exact locations where the Apollo 17 astronauts acquired panoramic image sequences while they were on the lunar surface in December 1972. For this, we analyzed the historical (Hasselblad) astronaut images together with current high-resolution images from the Lunar Reconnaissance Orbiter Camera (LROC), which we generated into 3-D elevation models and geodetic maps. We used a traditional geodetic method to determine the astronauts' positions during image acquisition by measuring the directions to lunar landmarks (control points) shown in their photographs. The positioned astronaut images were then used for further image analysis. Our cartographic analysis resulted in a map of the Taurus-Littrow valley covering the complete Apollo 17 exploration site, as well as a series of large-scale maps for all of the major geology stops.

## 1. Introduction

High-resolution images at pixel scales of 25–50 cm acquired by the Lunar Reconnaissance Orbiter Camera (LROC) Narrow Angle Camera (NAC; Robinson et al., 2010) of the current Lunar Reconnaissance Orbiter (LRO) mission (Keller et al., 2016) provide the means to have a closer look at the exploration sites and the invaluable *on-site* measurements obtained by the Apollo astronauts. Recordings of the Apollo Lunar Surface Experiment Package (ALSEP), rock samples, photographs, and astronaut descriptions were evaluated at that time and are still very important sources of our understanding of the geology of the Moon. Regarding cartography, up to the present day, the Apollo 17 Traverses Lunar Photomap (Defense Mapping Agency, 1975), as well as the map-like station sketches provided by Mühlberger et al. (1973) in the Apollo 17 Preliminary Science Report are the most widely known reconstructions of the astronaut traverse path and their activities at the nine major geology stops.

By integrating recent orbital data sets in the reanalysis of historic Apollo data and by using computer-aided and state-of-the-art methods, high-resolution cartographic products and data analysis that depend on accurate geolocation can be improved significantly. Recently, LROC imagery is used by various research groups to *revisit* lunar landing sites to take a closer look at the exploration sites and to reevaluate the historic data in a wider and improved context. For example, by reevaluating his own on-site field observations from today's perspective and by integrating recent remote sensing data, Schmitt et al. (2017) draw new conclusions on the geological evolution of the Taurus-Littrow Valley. They also demonstrated the potential

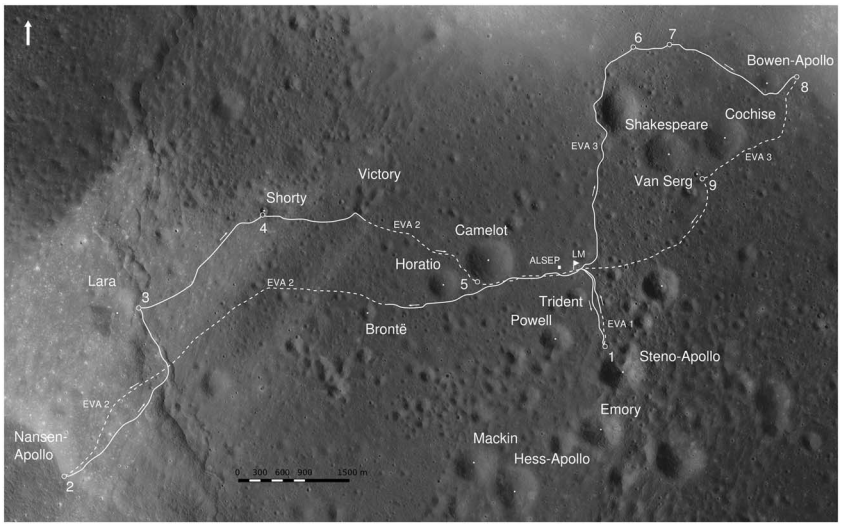


**Figure 1.** Major geology stations (numbered circles) and Lunar Roving Vehicle (LRV) traverses of the Apollo 17 crew. The traverse path was adopted from the traverse map of the Apollo era (Defense Mapping Agency, 1975; solid line: based on Very Long Baseline Interferometry observations; Salzberg, 1973; dashed line: approximate track).

of applying close-range photogrammetry to Hasselblad stereo images by creating a 3-D scene and deriving the geologic setting of collected and returned samples. By photogrammetrically analyzing a large set of surface images taken by the Apollo 11 crew, Pustynski and Jones (2014) created a landing site map, which was in good agreement with LROC NAC images when overlaid for comparison. Based on orthorectified LROC NAC images, Wagner et al. (2016) provide a comprehensive compilation of anthropogenic features on the entire Moon, and Karachevtseva et al. (2013, 2017) used LROC NAC orthoimages to map the traverse paths of the remotely controlled Lunokhod-1 and -2 rovers. The mentioned studies have in common that their analyses are based either on astronaut images only or on orbital images only. The work presented here is a joint analysis of close-range surface images and orbital images.

Previously, we reported on our cartographic study of the Apollo 17 landing site, in which we derived astronaut and feature positions by analyzing Apollo surface panoramas in combination with LROC NAC orthoimages (Haase et al., 2012). We used fully assembled Hasselblad panoramas provided by the Apollo Lunar Surface Journal (ALSJ; https://www.hq.nasa.gov/alsj/) to measure networks of directions to prominent lunar landmarks. Camera positions were determined by applying (2-D) network adjustments. At that time our investigation was limited to a relatively small area of 3.2 $km^2$ near the Lunar Module (LM) descent stage, the ALSEP site, and Traverse Station 1 (see Figure 1) for lack of a high-resolution digital terrain model (DTM), not to mention an orthomosaic covering the remaining area.

By now the complete Apollo 17 landing site has been imaged by the LROC NAC multiple times, under different lighting conditions, at high resolutions of 25- to 50-cm pixel scales, and providing geometric stereo imagery. This allowed us to generate a larger DTM and orthomosaic and extend our cartographic investigation to cover the entire region the astronauts explored during their three Extra-Vehicular Activities (EVA).

For all of the astronauts' preplanned sampling stops, the so-called *traverse stations*, we determined the positions from where station panoramas were taken and, based on that, geolocations of prominent surface features. Following the historic Apollo 17 station maps (Mühlberger et al., 1973), for each of the nine traverse stations, we created large-scale (orthoimage) maps. In addition, to give an overview of the entire exploration area the astronauts navigated, we generated a new "*Apollo 17 Landing Site* map at a scale of 1:15000 including the astronauts' traverse path, nomenclature, and elevation contours (section 3.4).

To specifically map the ALSEP area, a high-resolution LROC NAC image providing a ground pixel size of 25 cm was used. Previously, various research groups visually inspected and interpreted single features captured in the NAC images as astronaut equipment. This visual approach bears the risk of misinterpretation, and besides, some of the instruments are too small to be resolved in the orbital images, for example, antennas or the geophones inserted in the upper regolith and marked with red flags. To unmistakably identify the

**Figure 2.** The *West Pan* of Traverse Station 5 was acquired by astronaut Cernan on the southwest rim of Camelot Crater (panorama assembled by W. Harold from Johnson Space Center, source: Apollo Lunar Surface Journal [ALSJ]).

ALSEP instruments and to provide accurate coordinates of the complete suite of instruments, we used Hasselblad stereo images allowing us to carry out geodetic triangulation. At the ALSEP site we achieved accuracies for panorama and instrument positions of ±0.5 m and better.

## 2. Material and Methods

To document their field geology work and for postflight surveying purposes, the Apollo 17 astronauts Eugene Cernan and Harrison Schmitt took 2,218 photographs on the lunar surface (Apollo 17 Mission Evaluation Team, 1973). Using two metric Hasselblad cameras (see section 2.2), they recorded single frames, stereo pairs, and series of overlapping photographs to form panoramas. At each major sampling stop along their traverse path (except for Station 3) they acquired at least two full panoramas to enable their location to later be determined. They would stand in one position and turn around while taking a sequence of at least 15 Hasselblad frames at regular intervals to cover a 360° field of view (see Figure 2 for an assembled version of a station panorama).

These images not only provide unique close-up views of the lunar surface but also allow making angular measurements, which can be used to derive positions, feature sizes, directions, and distances. We applied (2-D) least squares network adjustments to derive the positions from where the astronauts acquired images. Unlike our previous approach (Haase et al., 2012) of using preassembled full panoramas provided by the ALSJ, we here used single Hasselblad frames to avoid image distortions possibly introduced by *stitching* the images together during panorama production. Instead, we determined single-camera positions of individual Hasselblad frames and derived a mean position from where panoramas were taken.

### 2.1. LROC NAC Image Data

LROC's NAC consists of two monochrome charge-coupled device line-scan imagers (~5,000 pixels), NAC-L and NAC-R, which are aligned side by side with a small overlap to provide a twice-as-wide field of view (FOV) of 2 × 2.85° in the cross-track direction. From the nominal orbit altitude of 50 km the twin NACs provide a ground pixel size of 0.5 m. A combined NAC-L/R-mosaic covers a ground track swath of about 5 km and typically 26 km in length. Stereo imagery is acquired from adjacent orbits by slewing LRO up to 30° off nadir to either side in the cross-track direction. During a 1-month period in August 2011, the orbit of LRO was lowered to approach the lunar surface as close as 22 km. The goal was to obtain images of the Apollo landing sites at highest ground resolution. Image mosaic M168000580L/R, which covers a 2.5-km-wide swath at the immediate Apollo 17 landing site, was obtained during that time and provides a pixel size of 25 cm × 56 cm. A NAC-L/R orthomosaic of that image was resampled to 25 cm/pixel and used to map the ALSEP site and the area surrounding the LM.

To generate high-resolution 3-D products and orthoimages from LROC NAC images, we used a modified version of the photogrammetric processing software system developed at the German Aerospace Center (DLR) for the automated and systematic processing of Mars Express High Resolution Stereo Camera (MEX HRSC) image data (Scholten et al., 2005, 2012). The underlying programming platform of the DLR stereo-processing pipeline is the Video Image Communication and Retrieval (VICAR) Image Processing System (National Aeronautics and Space Administration, 2018). As a first step, all LROC NAC images at Experiment Data Records (EDR) level were converted from the Planetary Data System (PDS) to VICAR's own image file format and were then radiometrically calibrated using the calibration files provided by the LROC team.

#### 2.1.1. Photogrammetric LROC NAC DTM Processing

Four NAC stereo pairs at pixel scales of 0.5 m and stereo angles ranging from about 25° to 30° are the image base of the Apollo 17 DTM used within this study. A 200-m-wide gap extending in the along-track direction at 30.7°E was filled using a stereo image pair with lower image resolution (1.0 m/pixel) and low stereo quality. Image names and selected image parameters are listed in Table A1 in Appendix A.

#### 2.1.1.1. SPICE Kernels

To determine the parameters of the camera's exterior orientation (position and pointing), we used the Navigation and Ancillary Information Facility (NAIF) SPICE kernels (Acton, 1996) provided by the NAIF team at the Jet Propulsion Laboratory and the LRO Mission Operation Center at Goddard Space Flight Center. These files provide ancillary information about the spacecraft clock, spacecraft and target positions and orientations, target size and shape, and reference frames.

Instead of the spacecraft's nominal trajectory, we used the refined *Spacecraft and Planet Kernels* (spk) provided by the Lunar Orbiter Laser Altimeter (LOLA) science team (Mazarico et al., 2012, 2013). Besides LRO radio tracking data, these kernels incorporate LOLA crossover adjusted positions, Earth-based laser ranging, and the lunar gravity field solution GRGM900C provided by the Gravity Recovery And Interior Laboratory (GRAIL) science team (Lemoine et al., 2014). Furthermore, we made use of the refined C-matrix kernels (ck) provided by the LROC operations team at the Arizona State University (Speyerer et al., 2014), which include variations in the alignment of the twin NACs induced by temperature changes in orbit. A complete list of the SPICE kernels used to compute exterior orientations are listed in Table A2 in Appendix A.

#### 2.1.1.2. Iterative DTM Processing

A typical LROC NAC stereo-image set is acquired by two sensors (NAC-L and NAC-R) from two different orbits and thus consists of four images. This constellation allows for up to four different stereo combinations (L-L, R-R, L-R, and R-L) resulting in a maximum of four individual surface models, which are combined to one DTM. Ultimately, the number of stereo combinations depends on the local topography and the degree of image overlap and typically amounts to three or four. To derive 3-D topography, we used the DLR stereo processing chain (Scholten et al., 2005), which is composed of three main steps: (1) determination of a dense grid of conjugate points for the entire stereo model; (2) forward ray intersection based on the matched image points, camera interior orientations, and exterior orientations (resulting in 3-D ground points); and (3) DTM interpolation.

The extraction of an accurate and dense net of image tie points from a stereo-pair is the most crucial factor within DTM generation. We used the DLR area-based multi-image matcher, which uses prerectified images in identical map projections and constant pixel scales to reduce and harmonize parallax effects. This keeps the search areas for the matching algorithm small, and thus, reduces the number of mismatches. After the image matching process, the image coordinates of the tie points are transformed back to line and sample coordinates of the original images using transformation files stored during the prerectification procedure. This step is essential, because the SPICE-based orientation data are rigidly associated with the image geometry at the time of image acquisition.

As prerectification requires topographic data, the processing of the DTM is done in an iterative procedure. In a stepwise manner, based on an initial DTM of the best available quality and grid size, at first, a low-resolution and smoothed LROC NAC DTM is created, which is gradually improved and densified during further iterations. As initial terrain we used a DTM of a raster grid of 8 m based on Kaguya/SELENE Terrain Camera (TC) images (Haruyama et al., 2014). Comparable to a pyramidal approach, the pixel scale of the prerectified images was chosen relative to the grid size of the DTM used for prerectification (~1/4), respectively, to keep the effects of parallax (and thus the search areas) small. In prerectified LROC NAC images the parallax caused by inaccurate terrain elevation occurs in the cross-track direction (sample), while errors in the exterior orientation have an effect predominantly in flight direction (line).

Within the first iteration, images were prerectified to 2 m/pixel, at which scale parallaxes are due to improper elevation rather than inaccurate exterior orientation. The effect of the latter increased with every step of the iteration, concurrent with the increase in the chosen image resolution. While the DTMs were improved and the sample-parallaxes gradually became smaller, the line-parallax caused by errors in the position and pointing information reached its maximum effect (up to 7–8 pixels) at the final iteration level with prerectified images of 0.5 m pixel scale.

The image matching is based on an area-based correlation followed by a least squares matching providing conjugate points with subpixel accuracy (Wewel, 1996). After back-transforming the matched image points to original line and sample coordinates, we determined object points in the body-fixed Moon-Earth/Polar-Axis frame as well as relative accuracies by applying forward ray intersection for each of these tie points. After that, a map referenced LROC NAC raster DTM was generated in a VICAR 16-bit signed short integer image format. The vertical resolution is 0.1 m, and elevations are related to a sphere with a radius of

**Table 1**
*Mean Relative Point Accuracies of the Five NAC DTM Strips, Which Were Combined to One Final DTM*

| LROC NAC stereo pair | Mean 3-D forward ray intersection accuracy (m) | | | |
|---|---|---|---|---|
| Orbit 1/orbit 2 | L-L | R-R | L-R | R-L |
| 5374/5375 | 0.14 | 0.33 | 0.76 | 0.99 |
| 8676/8677 | 2.46 | 0.53 | 1.59 | 0.27 |
| 13104/13105 | - | - | - | 6.94 |
| 5026/5027 | 1.23 | 0.70 | 0.14 | 0.42 |
| 7633/7634 | 0.2 | 0.45 | 0.25 | 0.52 |

*Note.* DTM, digital terrain model; LROC, Lunar Reconnaissance Orbiter Camera; NAC, Narrow Angle Camera.

1737.4 km. At each iteration level the DTM raster grid was chosen according to the previous iteration's prerectification scale (DTM scale = prerectified image scale × 3), starting from 6 m/pixel to a final raster grid of 1.5 m/pixel.

As map projection of the near equatorial location of the Apollo 17 site we chose the Transverse Mercator projection with true scale at 30.7°E (central meridian) to keep distortions small. A sphere with a radius of 1,737.4 km served as reference body for the map projection. Only object points within the 1σ range of the stereo-pairs' individual mean point accuracy were included in the DTM interpolation. See Table 1 for mean relative inter-stereo forward ray intersection accuracies of the final DTM. Because of its low stereo angle of $<10°$ the stereo pair acquired from orbits 13104/13105 has a relatively low mean 3-D accuracy resulting in less accurate object points. However, none of the geolocations determined in this study are located within this 200-m-wide area, implying that none of the elevations provided are affected by this reduced accuracy.

The stereo images used for DTM processing were orthorectified and map-projected to a uniform pixel scale of 0.5 m based on the generated LROC NAC DTM strips, the exterior orientations, and the calibrated parameters of the sensor model (interior orientation). The same map projection as for the DTM strips was chosen (Transverse Mercator with central meridian at 30.7°E). Inaccurate exterior orientations of the individual images result in errors of the absolute position of the DTM/orthoimage sets. After generating an orthomosaic these discrepancies vividly show up at the image edges, for example, where surface features may appear twice because of lateral offsets. The vertical component of positional errors are reflected in DTMs by low forward ray intersection accuracies and offsets in elevation, creating discrepancies in terrain edges in the along-track direction where two surface models overlap.

To account for these positional discrepancies, we applied corrections in two separate steps. First, we improved the relative accuracy of the orthoimages (in 2-D) and the single DTM strips (in 3-D) to achieve internally consistent surface representations of the whole investigation area. In a second step the two surface models were then referenced to adequate lunar reference frames to improve their positional (absolute) accuracies.

#### 2.1.1.2.1. Improving the Internal, Relative Accuracy

Using one centrally located image as initial control, we accounted for lateral inconsistencies by successively referencing adjacent image strips from the center of the area outwards to the west and to the east. For this, we determined lateral offset values (in image line and sample) in the overlapping orthoimages, which were then manually corrected for. All orthorectified images of the stereo pairs used for DTM processing were referenced to image M134991788L (orbit 5027), which covers the central part of the Taurus-Littrow Valley including the LM and the ALSEP central station. After improving the relative accuracy of the orthoimages they were merged to a preliminary orthomosaic. The images used to create this preliminary mosaic were chosen only because of their direct relation to the corresponding DTM by sharing the same projection geometries. The strong correlation of a DTM/orthoimage set derived from identical images allows transferring the determined horizontal corrections to the related DTM. It also keeps lateral displacements during orthorectification due to errors in elevation to a minimum. The previously determined lateral corrections were applied to the related DTMs after scaling them to the appropriate pixel size. However, to create high-quality cartographic products, additional criteria besides their geometrical consistency need to be taken into consideration when selecting images for a mosaic. To achieve a uniformly illuminated and radiometrically adjusted orthomosaic, we substituted some of the original images used for DTM processing in a subsequent step, as described in the following section.

To further correct the DTMs for the vertical effects of errors in the exterior orientation, we determined mean offsets in elevation where adjacent DTMs overlap. The same strategy as for the lateral corrections described above was applied, again using stereo model 5026/5027 as reference and proceed toward the western and eastern boundaries of the DTM. We applied vertical shifts ranging from −3.6 to +4.1 m to improve the relative accuracy of the five elevation models, which were then combined to one DTM.

#### 2.1.1.2.2. Improving the Absolute Accuracy

To improve the absolute position of the orthomosaic and the DTM, we used a combination of the two currently most accurate reference frames of the Moon by breaking it down to a horizontal and vertical control.

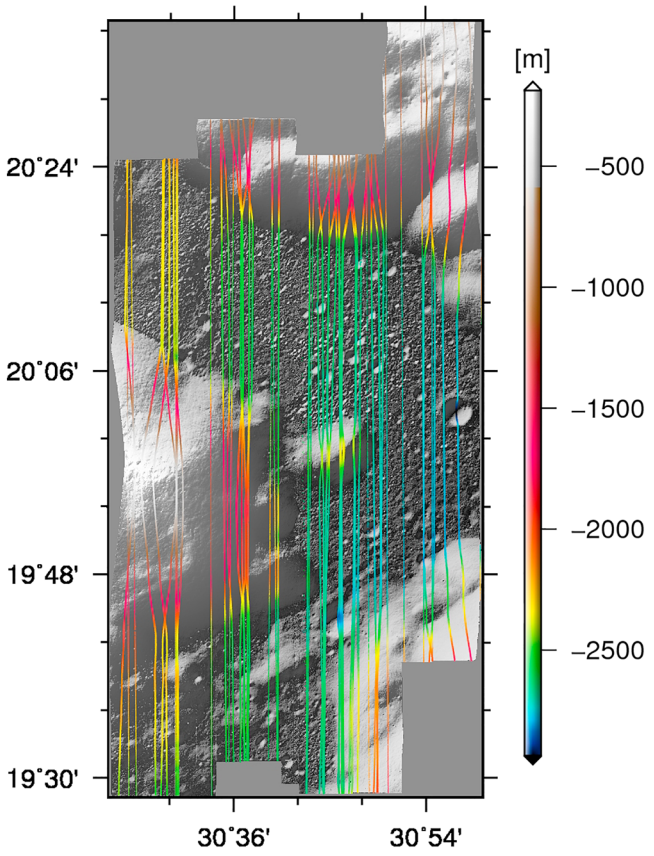


**Figure 3.** Overlay of 47 color-coded Lunar Orbiter Laser Altimeter (LOLA) tracks on the shaded Lunar Reconnaissance Orbiter Camera (LROC) Narrow Angle Camera (NAC) digital terrain model (1.5-m grid) of the Apollo 17 landing site (after coregistration). Color-coded elevations are given relative to the mean lunar radius of 1,737.4 km.

Horizontally, we controlled our surface models to the fundamental Lunar Geodetic Network, which is characterized by best available, fixed coordinates that were assigned to unique features on the lunar surface. Here the control points are of human-made nature and are defined by five Lunar Laser Ranging (LLR) reflectors and five ALSEP transmitters whose locations were determined by laser altimetry and Very Long Baseline Interferometry (VLBI). Davies and Colvin (2000) provided Mean-Earth/Polar-Axis (ME) coordinates of the Apollo 17 ALSEP radio transmitter housed by the ALSEP Central Station (C/S), which can be identified in one of the images (M134985003L, orbit 5026). By following the above described conventional way of referencing, the coordinates provided in this document are consistent and comparable to already existing and established data sets. To agree with the coordinates given by Davies and Colvin (2000), the LROC NAC orthomosaic and DTM had to be shifted by 15.0 m west and 6.5 m south. The horizontal accuracy of the ALSEP transmitter coordinates were estimated to about ±10 m (King et al., 1976), which consequently is propagated to the coordinates determined in this study. In case new values with improved absolute accuracy become available in the future, whose quality and sole use is commonly agreed on, the complete data set can easily be rereferenced by a simple coordinate transformation.

To exploit the high radial accuracy of the recent LOLA data set of ~1 m (Mazarico et al., 2013), we selected 47 crossover improved LOLA tracks to be used as vertical control. The coregistration technique developed by Gläser et al. (2013) was applied to determine a best fit of the SPICE-based DTM relative to the LOLA frame. Figure 3 shows the distribution of the selected, coregistered LOLA tracks in the study area. Lateral offsets of the DTM were 1.5 m in the western and 1.5 m in the southern direction, which is equivalent to one DTM pixel. Nevertheless, these offsets were not incorporated in favor of the LLR/VLBI frame.

To account for the determined vertical offset, however, the horizontally controlled DTM was raised by 6.7 m to fit to the LOLA reference frame. For comparison, if we had chosen to vertically reference the DTM to the radius value of the C/S given by Davies and Colvin (2000), the DTM would have to be raised by 42.8 m instead. Here the discrepancy of about 36 m between the LOLA grid and the radius of the C/S given by Davies and Colvin (2000) confirms the conservative estimate of ±30 m (King et al., 1976) of the vertical error. Afterward, the standard deviation of the elevation differences of the 47 LOLA profiles and the corresponding elevations of the controlled NAC DTM was ±1.3 m. This is assumed to primarily result from remaining northwest trending tilts of the individual NAC DTM strips, which were not entirely removed by our method.

#### 2.1.2. LROC NAC Controlled Orthomosaic

The orthomosaic used in this study for taking measurements and creating cartographic products of the Taurus-Littrow Valley consists of 10 LROC NAC images. The criteria after which the individual images were chosen were as follows (sorted by priority): light coming from the west in addition to similar incidence angles to achieve homogeneous illumination conditions, a ground pixel size not exceeding 0.5 m, and favorably nadir imagery to minimize possible feature displacements caused by elevations differences.

Five images previously used for DTM processing located at the outer boundaries of the investigation area met at least the first two prerequisites. The innermost images of the preliminary 0.5 m/pixel orthomosaic, which were processed along with the DTM, had to be substituted, because of opposite illumination (Sun direction) or insufficient image scale (see the last column in Table A1 in Appendix A). Nadir imagery with the Sun shining from the west was not available throughout the area.

Images M168000580-L and -R (orbit 9892), which were recorded during the 1-month low-orbit period, cover the area in close proximity to the LM including the ALSEP area. Both images were orthorectified using an

adapted version of the DTM, which was horizontally shifted to reasonably match the image's projection geometry in order to minimize pixel displacement caused by faulty terrain. The generated orthoimages were resampled to match the 0.5-m pixel scale of the final orthomosaic, controlled to the ALSEP central station and integrated into the preliminary mosaic. Three additional images covering the area west of the landing site were rectified accordingly and referenced to the adjacent (controlled) orthoimage, working outward from the center image. Names and selected characteristic parameters of the images used for the final orthomosaic are listed in Table A3 in Appendix A. They are listed in the order of layering, the first image being displayed in its full east-west extent on the top and the image listed last being displayed on the bottom layer partially covered by overlying images.

To merge the geometrically corrected orthoimages into a mosaic, the DLR radiometric mosaicing tool was used. It is capable of adjusting the brightness of adjacent, overlapping images and to produce seamless transitions from image to image by weighted averaging of overlapping image parts (Scholten et al., 2005).

### 2.2. Hasselblad Surface Imagery

While performing EVAs, the astronauts were equipped with two electronically powered Hasselblad 500 EL Data Cameras, which were typically attached to the chest of their spacesuits to enable two handed operations and to provide some support to the camera. The Hasselblad Data series consisted of metric cameras modified for use under space conditions, accurately calibrated and equipped with a high-precision Réseau plate in front of the image plane (Kammerer & Zeiss, 1972) to provide photogrammetric information in the analysis of the photography. The Réseau grid, that is, 5 × 5 crosses at 10-mm intervals, is imaged in each Hasselblad frame (70-mm film) and defines the image coordinate system. The cameras were fitted with Zeiss Biogon f/5.6 moderate wide-angle lenses (60-mm focal length) specifically designed for the National Aeronautics and Space Administration (NASA) with rigid demands for minimal distortion. The Hasselblad cameras were left behind on the lunar surface; only the film magazines were brought back to Earth. The film rolls were developed and since then they are stored (deep-frozen for most of the time) at the Johnson Space Center, not allowed to leave the building.

We used two different online sources to obtain astronaut imagery. The majority of Hasselblad image files we used were downloaded from the ALSJ. Supported by the NASA History Office, this website comprehensively documents the Apollo missions and provides digitized Hasselblad image files along with the supporting information. The images provided on this website are original film scans obtained from the Johnson Space Center that were reduced to an image size of 2,340 × 2,350 pixels (~1,150 dpi) and edited before putting them online. By means of the Réseau grid we determined a mean pixel size of 22 μm. Whenever possible, we downloaded Hasselblad frames provided by the *Apollo Image Archive* (http://tothemoon.ser.asu.edu/gallery/apollo). To preserve the invaluable Apollo photography and to allow researchers and the general public free access to digitized versions of the originally flown film, the Johnson Space Center and the School of Earth and Space Exploration at the Arizona State University are currently scanning the Apollo flight films at very high resolution and extended bit depth (Lawrence et al., 2008). At the time of our analysis, though, the Apollo 17 Hasselblad scans were not completely available yet.

#### 2.2.1. Hasselblad Camera Model and Distortion

To make use of angular measurements made in photographs, the geometry of the corresponding camera (interior orientation) has to be known to a sufficient degree. All the Apollo cameras flown to the moon were carefully calibrated before flight (Borgeson & Batson, 1969), and the parameters, that is, the location of the principal point, the principal distance, and the magnitude and direction of the camera lens distortion, were recorded in mission calibration reports. The optics of both Hasselblad cameras flown on Apollo 17 were analyzed in preparation of earlier missions (for future use). One of the Apollo 17 surface cameras (S/N 1023), which was primarily used for color imagery taken by E. Cernan, was calibrated in preparation of the Apollo 16 mission (Malhotra, 1972). The calibrated parameters of the interior orientation of the second Hasselblad camera (S/N 1032), which was mainly used by astronaut H. Schmitt, were not available to us.

Instead of using only one focus at infinity, as it is common for metric cameras, the Hasselblads were used at several focus settings, each time bringing about a change in the optics, that is, changing the lens-to-image plane distance (principal distance). Prior to image acquisition the astronauts had to estimate the distance to the target, rate it near, medium, or far, and adjust the focus setting accordingly. Three discrete focus distances were uniquely marked with a *click-stop*. The calibrated principal distances for

these three detents and lens distortions were recorded in the calibration report prior to the mission. Camera S/N 1023 was calibrated at focus distances of 6, 10, and 50 foot resulting in values of the calibrated principal distances of 63.0, 62.3, and 61.4 mm, respectively. The principal distance has great influence on position determination by providing the ratio for transforming between image and object scale. Here a change of 0.1 mm in the principal distance results in a 0.5-m offset along the principal visual ray.

Contrary to the recorded values given in the calibration report, in the available mission transcripts of the EVAs the astronauts commonly referred to *5-foot*, *15-foot*, or *74-foot* focus settings. The latter was the preferred setting used for station panoramas as can be seen in the communication transcripts. To begin with, we associated the *74-foot* focus setting with the calibrated values of the detent setting of 50 foot. By analyzing several frames of *standard 74-foot* panoramas we achieved best results by applying a principal distance of 61.5 mm, with lowest discrepancies between the individually determined camera positions belonging to the same panorama sequence. We applied no corrections for the principal point position nor the radial lens distortion because of negligibly small calibrated values.

Image distortion resulting from film deformation, unevenness or scanning was taken into account by means of the Réseau. We measured the centers of the Réseau crosses with a precision of ±1 pixel, and the maximum pixel dislocation resulted in ±2 pixels, occurring, if at all, mainly at the image edges.

### 2.3. Method

In principal, the approach used in this study is the same as was used during the Apollo era, the traditional surveying method of *three-point resection*". Here computer-aided least squares adjustment supersedes tracing paper to fit local networks of angular directions to prominent lunar landmarks, and orbital photographs are replaced by digital, high-resolution orthomaps from recent lunar missions.

To determine the position of the camera perspective center of a Hasselblad frame, we measured image coordinates of several (as many as possible) surface features for each frame. The Hasselblad Réseau was used to transform between pixel coordinates and metric image coordinates. Their horizontal components were then converted to angular directions incorporating the camera's principal distance. The same features had to be identified in the LROC NAC orthomap to provide reference coordinates with respect to the coordinate system of the orthomap. For each panorama site we resampled the original 0.5 m/pixel LROC NAC orthomosaic and map-projected it to a local stereographic projection, defining the center at the approximate position of the astronaut during image acquisition. By doing so, we preserved directions from the origin of the map, which is necessary for correlating the measured angles with the local coordinate system of the mosaic and for plotting the network of angles onto the orthomosaic.

To improve the leveling of some of the images to come as close as possible to our assumption of measuring horizontal angles, we utilized an assembled panorama of that same scene (provided by the ALSJ) and rotated the particular frame about its center Réseau cross to fit the scenery. We primarily applied this procedure to images that were taken from the seat of the rover or while standing on a steep slope. As an example, Figure 4a shows a single frame of a *rover pan* that was acquired by astronaut Schmitt to document the deployment site of EP-1 at Victory Crater. This particular frame was rotated by 14° before measuring angular directions.

The observed angles were then adjusted to the ground control points within a least squares adjustment. The functional model of a network adjustment is given by the fundamental direction observation equation:

$$D_{CF} + v_{CF} = Az_{CF} + \omega_C = \arctan\left(\frac{x_F - x_C}{y_F - y_C}\right) + \omega_C$$

| | |
|---|---|
| $D_{CF}$ | observed angular direction from the camera's position $C$ to a surface feature $F$ |
| $v_{CF}$ | residual in the observed angle $D_{CF}$ |
| $Az_{CF}$ | north azimuth of a surface feature $F$ |
| $\omega_C$ | unknown orientation angle toward north |
| $(x_C, y_C)$ | unknown 2-D coordinates of the camera's position $C$ |
| $(x_F, y_F)$ | known 2-D coordinates of a surface feature $F$ (control) |

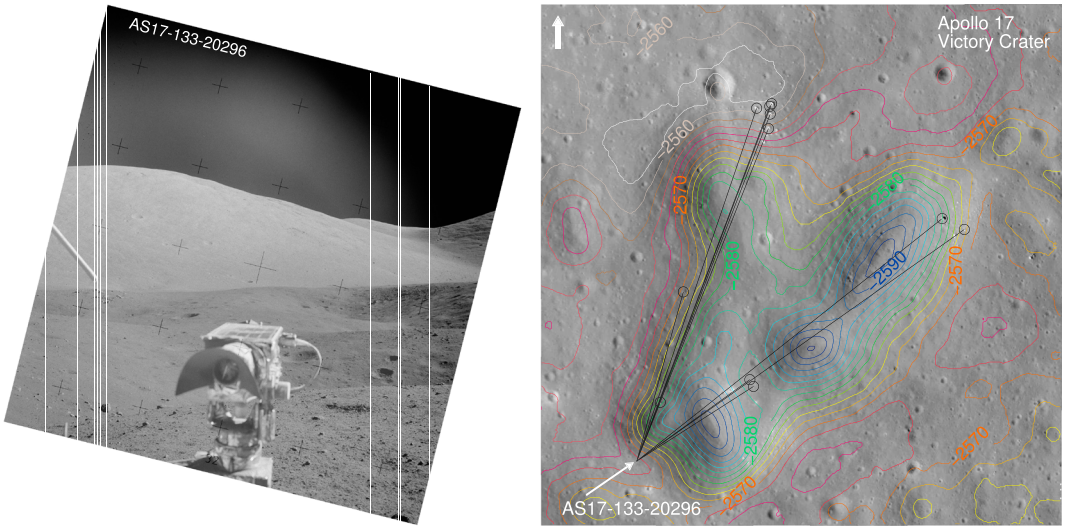


**Figure 4.** (a) To approximately level frame AS17-133-20296 horizontally it was rotated before measuring angular directions to reference features located within Victory Crater (horizontal directions are represented by white lines). (b) The measured network of angular directions (here represented as black lines emanating from the camera's perspective center) was adjusted to the corresponding points of reference (boulders circled in black). Color-coded contours were included to support better perception of topography.

A minimum of four observed directions $D_{CF}$ set up an overdetermined, nonlinear equation system, which is solved after linearization using a first-order Taylor series approximation. Feature identification and correct matching in both, the orbital and the on-site images, were supported by image plots of the angular network overlaid on the orthomap (see Figure 4b as well as Haase et al., 2012, for further details). These visual, first-order approximations also provided initial values for the unknowns of the adjustment.

Once a Hasselblad frame's position and orientation toward north was determined, these images were further exploited to determine geolocations of astronaut equipment imaged in the Hasselblad frames. By applying polar point determination or triangulation in case of available stereo views, these calculations were independent of whether or not a surface feature was visible in the LROC NAC orthomap.

In contrast to utilizing fully assembled 360° panoramas, as reported in Haase et al. (2012), we refined our analysis and used the original, single Hasselblad frames to determine individual astronaut or rather individual frame positions. In the case of a panoramic image series, as they were routinely recorded at the traverse stations, we derived a mean panorama position after determination of at least three camera positions of frames possibly aiming at most diverse viewing directions (de facto we used 9–10 frames per panorama site on average). In best cases, where control features were available in close vicinity, the individual frame positions differed by only 1–2 LROC NAC pixels at maximum. Because the cameras were attached to the front of the space suits, the focal points of the cameras are assumed to have moved in circles rather than about a point when panoramic images were taken. Owing to the turning and moving of the astronauts in combination with errors introduced by the assumption of accurately leveled image planes, which complies with the assumption of measuring horizontal angles, the independently determined camera positions slightly differ from one another by only a few NAC pixels.

Using fully assembled panoramas downloaded from the ALSJ in the first place had the appealing advantage of enabling us to measure direction angles to control points on a full 360° range within just one image (mosaic). The approach is comparable to a surveyor using an accurately leveled theodolite to measure horizontal directions for self-positioning. A leveled, geometrically correct 360° image would simplify the task of image orientation by the need of only four control features within a 360° FOV, instead of four control features per single frame (FOV ≈ 46°). It also takes just one calculation step to get a panorama position. On the other hand, a combined adjustment of all measured angular directions within the 360° view erroneously

**Table 2**
*ME Coordinates of the Panorama Stations of the ALSEP Site*

| Site | Longitude (°E) | Latitude (°N) | Radius (m) | *X* (m) | *Y* (m) | *Z* (m) |
|---|---|---|---|---|---|---|
| (Geo-3) Pan (S/N 1032, color) | 30.76515 | 20.19069 | 1,734,777.5 | 1,399,043.0 | 832,844.0 | 598,750.9 |
| (C/S) Pan (S/N 1032, color) | 30.76497 | 20.19218 | 1,734,777.7 | 1,399,032.3 | 832,831.8 | 598,793.4 |
| (North) Pan (S/N 1032, b&w) | 30.76464 | 20.19247 | 1,734,777.4 | 1,399,034.3 | 832,822.0 | 598,801.5 |

*Note*. ALSEP, Apollo Lunar Surface Experiment Package.

forces the network to have just one instead of various single origins and leads to inconsistencies and low inner accuracies. Distortions and errors, for example, feature duplications, introduced by geometrically inaccurate generation of the panoramic mosaics contributed to the decision to completely abandon the use of fully assembled panoramas of unknown processing and mosaicing methods. By adjusting angular measurements made in the original, unprocessed single frames we improved the inner accuracies of the angular networks and, thus, were able to halve the standard deviations we assigned to our measurements before adjustment. Feature coordinates derived from the LROC NAC orthomap were assigned to have an uncertainty of ±0.5 m (=image pixel size), and directions were observed in the Hasselblads with an accuracy of ±0.03° on average and ±0.2° at the lowest.

## 3. Results

Lateral coordinates determined in this study are relative to the ME coordinates of the ALSEP central station (30.76492°E, 20.19209°N) given by Davies and Colvin (2000). Except for the immediate landing site, control points needed for angular network adjustments were provided by the 0.5-m scale orthomosaic of the Taurus-Littrow Valley described in section 2.1.2. As for astronaut positioning at the LM and ALSEP site, we exploited image M168000580R acquired from LRO's low-orbit period. It was orthorectified, map-projected to local stereographic projection with its center at the respective panorama position, resampled to 0.25 m/pixel, and controlled to the C/S. When comparing our determined instrument positions with the orthoimage, some of the larger sized ALSEP instruments, that is, C/S, HFE, LACE, and LEAM (see Table A4 in Appendix A for a list of acronyms used throughout this study and in the provided maps), could be associated with features which were clearly distinguishable from the surrounding regolith. This fact not only confirmed but also refined our calculations by introducing these instruments as additional, close range and precisely measurable control points. Elevations are derived from the LROC NAC DTM, which was vertically coregistered to available LOLA profiles (see section 2.1.1). Unless stated otherwise in the following sections, we determined geolocations with (horizontal) accuracies of better than ±1 m.

### 3.1. Coordinates of the ALSEP Site

About 4 hr after arrival on the lunar surface on 11 December 1972 the Apollo 17 crew began EVA 1. Among their first tasks were to deploy the suite of ALSEP instruments, collect samples, and acquire photography. All three Hasselblad panoramas recorded at the ALSEP site located 195 m distant to the LM were taken by astronaut Schmitt. After completing ALSEP deployment he started photo documentation proceeding from south to north. First, he acquired a panorama standing between Geophone Rock and the Geo-3 instrument (frames AS17-147-22544 to AS17-147-22562). He then moved northward and recorded a second panorama standing right in the middle of the ALSEP instrument suite near the C/S. The frames are AS17-147-22569 to AS17-147-22588. Because of unfavorable imaging geometry in addition to using a noncalibrated (free) focus setting of about 15-foot, this panorama position has a reduced mean point error of ±0.9 m. After he had run out of film and had changed the film magazine (from color to b&w film), he acquired the northernmost panorama standing just outside the group of instruments. The third panorama consists of frames AS17-136-20683 to AS17-136-20710 and was then again taken at standard 74-foot focus setting. Except for the *C/S* Pan, the determined panorama positions have a mean point error of better than ±0.5 and are listed in Table 2.

Subsequent to panorama positioning we determined geolocations of the instruments captured in the Hasselblad frames by applying triangulation. For this we used stereo views provided by single frames of the northernmost and southernmost panoramas and photographs recorded at the geophone sites. Color photography proved to be very beneficial (if not essential) as far as being able to detect and identify small, distant instruments in the astronaut images, for example, the small, red geophone flags. We estimate the

**Table 3**
*ME Coordinates of the Apollo 17 ALSEP Instruments and Mission Relics*

| Instrument | Longitude (°E) | Latitude (°N) | Radius (m) | *X* (m) | *Y* (m) | *Z* (m) |
|---|---|---|---|---|---|---|
| C/S | 30.76492 | 20.19209 | 1,734,778.0 | 1,399,034.1 | 832,831.2 | 598,790.9 |
| RTG | 30.76503 | 20.19214 | 1,734,777.9 | 1,399,032.0 | 832,833.5 | 598,792.3 |
| HFE | 30.76497 | 20.19240 | 1,734,777.4 | 1,399,030.1 | 832,830.4 | 598,799.6 |
| LACE | 30.76536 | 20.19226 | 1,734,777.6 | 1,399,025.8 | 832,840.8 | 598,795.6 |
| LEAM | 30.76515 | 20.19191 | 1,734,777.8 | 1,399,032.2 | 832,837.6 | 598,785.8 |
| LSG | 30.76463 | 20.19221 | 1,734,778.0 | 1,399,037.2 | 832,823.4 | 598,794.4 |
| LSP | 30.76464 | 20.19236 | 1,734,777.8 | 1,399,035.6 | 832,822.8 | 598,798.6 |
| G/M | 30.76495 | 20.19177 | 1,734,777.9 | 1,399,036.5 | 832,833.5 | 598,781.8 |
| Geo-1 | 30.76669 | 20.19202 | 1,734,775.2 | 1,399,006.7 | 832,873.5 | 598,787.9 |
| Geo-2 | 30.76322 | 20.19147 | 1,734,779.3 | 1,399,065.3 | 832,793.7 | 598,773.8 |
| Geo-3 | 30.76510 | 20.19085 | 1,734,777.6 | 1,399,042.3 | 832,841.9 | 598,755.7 |
| Geo-4 | 30.76555 | 20.18902 | 1,734,777.0 | 1,399,051.6 | 832,862.5 | 598,703.4 |
| SEP | 30.77620 | 20.19179 | 1,734,773.2 | 1,398,868.9 | 833,105.8 | 598,780.8 |
| LM | 30.77168 | 20.19091 | 1,734,773.9 | 1,398,943.1 | 833,000.6 | 598,756.0 |
| LRV | 30.77634 | 20.18948 | 1,734,771.7 | 1,398,886.4 | 833,120.9 | 598,714.6 |
| Flag | 30.77149 | 20.19151 | 1,734,774.6 | 1,398,941.0 | 832,993.0 | 598,773.4 |

*Note.* The lateral coordinates of the Apollo Lunar Surface Experiment Package Central Station (ALSEP C/S) are consistent with the values provided by Davies and Colvin (2000). Radius values are derived from the Narrow Angle Camera (NAC) digital terrain model and are related to the Lunar Orbiter Laser Altimeter (LOLA) reference frame. See Table A4 in Appendix A for the use of acronyms.

determined positions of the astronaut equipment to be accurate to better than ±0.5 m. Their coordinates are listed in Table 3, and Figure 5 shows a large-scale map of all of the scientific instruments.

The Geophone module (G/M) was deployed 9.8 m south of the ALSEP central station. From there, the four identical geophones were laid out in a T-shaped pattern as shown in Figure 6. The distance between the LM and Geo-1 is 145.6 m (see Table A5 in Appendix A for source-receiver distances). Figure 7a illustrates distances and enclosed angles of the inner geometry of the geophone array. Except for the position of Geo-4, our results are in relatively good accordance with the layout of the geophone array given by Tanimoto

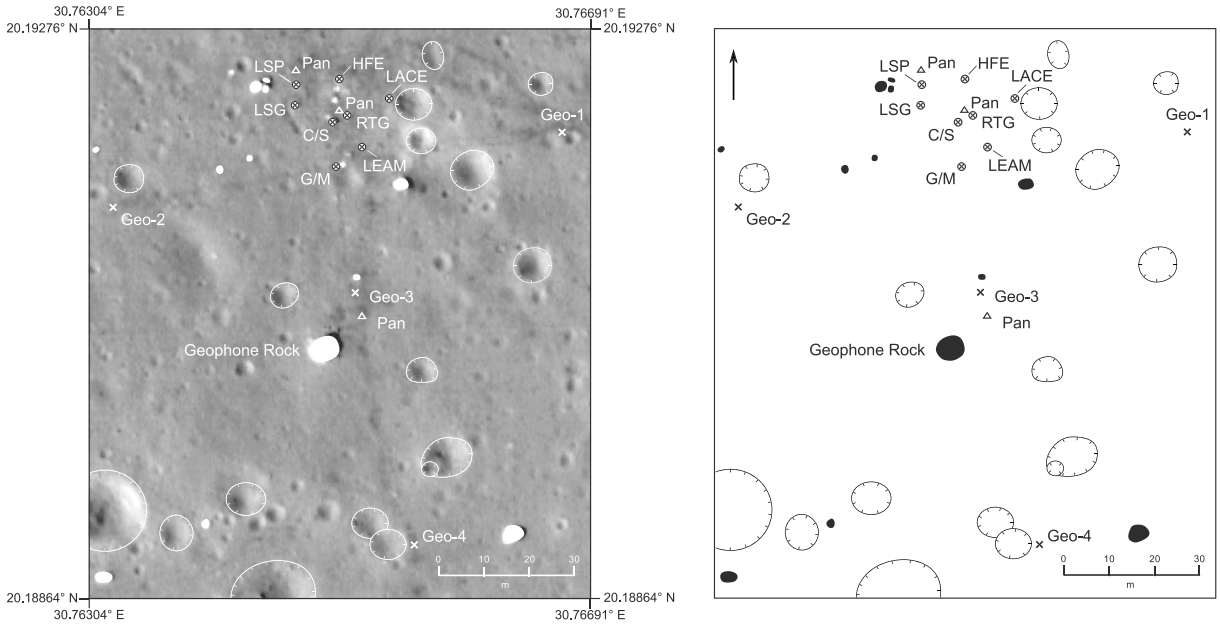


**Figure 5.** Controlled orthomap of the Apollo 17 Apollo Lunar Surface Experiment Package (ALSEP) site. (a) The astronauts' footprints between the ALSEP instruments are clearly visible in the image base (M168000580R, 0.25 m/pixel). Large rocks are mapped as white filled polygons, whereas craters are mapped with the white line feature. (b) Same map without image base and inverted color.

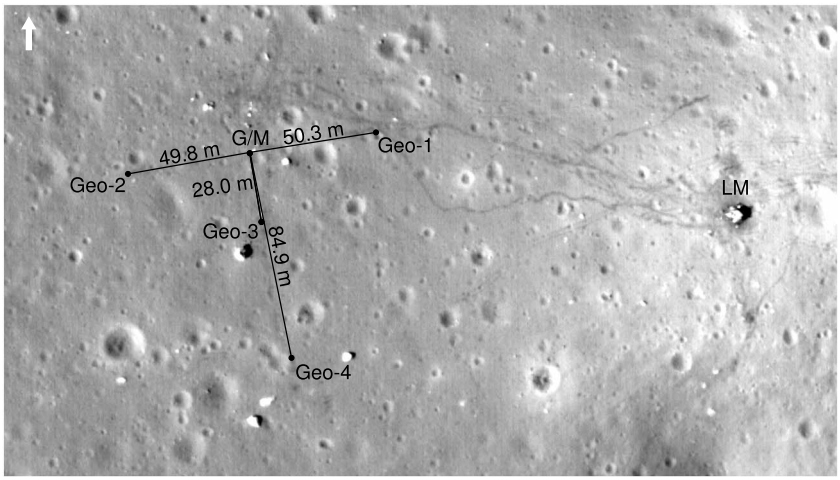


**Figure 6.** T-shaped layout of the four geophones at the Apollo 17 Apollo Lunar Surface Experiment Package (ALSEP) site. The Lunar Roving Vehicle (LRV) tracks and the crews' footprints are clearly visible in the 25-cm pixel scale Lunar Reconnaissance Orbiter Camera (LROC) Narrow Angle Camera (NAC) orthoimage (M168000580R).

et al. (2008; see Figure 7b). We determined the deployment site of Geo-4 to be about 8 m further to the northwest.

### 3.2. Coordinates and Maps of the Apollo 17 Traverse Stations

#### 3.2.1. EVA 1

Subsequent to the deployment of the ALSEP, the astronauts set off to their first geologic traverse. After a 13-min drive they arrived at Station 1 (Apollo 17 Mission Evaluation Team, 1973). We created a profile of the EVA 1 traverse and measured the length of the driven route between the LM and Station 1 to be 1,258 m. This implies an average velocity of about 5.8 km/hr. After 33 min of field work, including deployment of EP-6, they departed from Station 1 and returned back to the LM on a similar route as on their outward trip. After the crew had traveled 470 m they deployed explosive charge EP-7 en route, performed a rover pan to document the deployment site, and then continued driving. It took them about 14 min at an average speed of 5.4 km/hr to return back to the SEP site. The profile displayed in Figure 8 shows elevations of −2,626.2 m at its highest and −2,639.8 m at its lowest point, and the distance traveled by the astronauts at EVA 1 amounts to 2,530 m

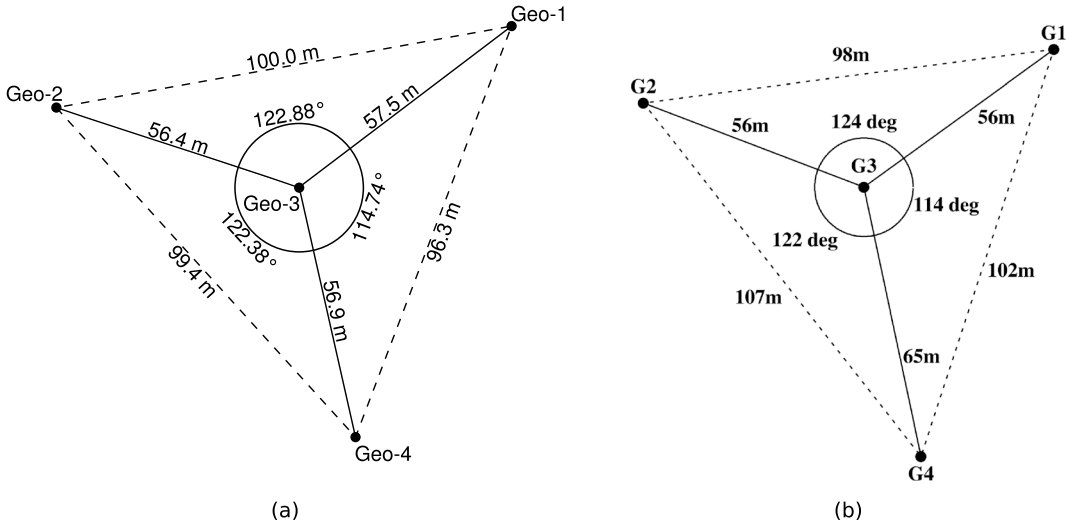


**Figure 7.** Geometry of the Apollo 17 Lunar Seismic Profiling Experiment (LSPE) geophone array. Comparing the layout (a) determined in this study with the layout (b) provided by Tanimoto et al. (2008), we determined the position of Geo-4 to be about 8 m further to the northwest.

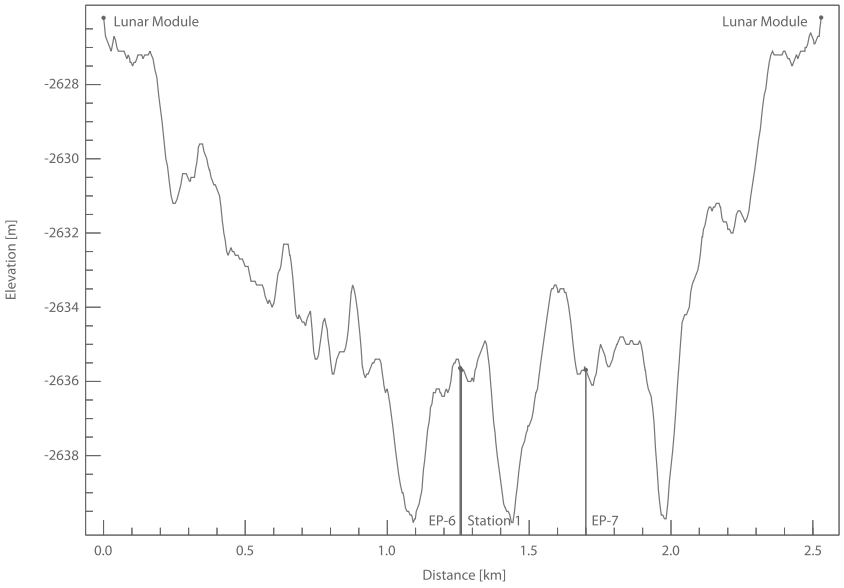


**Figure 8.** Apollo 17 EVA 1 profile. The maximum difference in elevation along the astronauts' route is 13.6 m.

in total. This agrees very well with the crew's odometer reading at the end of the traverse of 2.5 km provided by the report on the LRV Navigation System Performance (Smith & Mastin, 1973). The individual length of the traveled routes between stations, travel times, and derived average velocities are listed in Table 4. The latter are approximate only, because of minor stops and en route charge deployment, whose durations were not recorded and, hence, are not considered in our calculations.

#### 3.2.1.1. Station 1

Station 1 is located 1,114 m to the south of the LM in a gently rolling terrain about 150 m northwest from the crest of the Steno crater rim. Originally, Station 1 was planned to be at the east rim of Emory Crater, a drive of about another kilometer further south, but because of shortage of time the crew selected a small crater 12 m in diameter as their first sample stop instead. The science objectives for the originally planned Station 1 were to characterize the rock types of the subfloor and mantle units, as well as to investigate the contact relations exposed in the crater rim and wall (Wolfe et al., 1981). Activities at this station include a traverse gravimeter measurement, collection of rake samples, explosive charge deployment (EP-6), and photography.

Two panoramas were taken at Station 1. Astronaut Cernan acquired a panorama from east of the LRV (frames AS17-134-20408 to AS17-134-20431) and astronaut Schmitt from west of the LRV (frames AS17-136-20744 to AS17-136-20776; see Figure 9). Both panoramas were acquired after EP-6 had been deployed 3 m north of the LRV (center), and both astronauts were standing in direct line of sight to the EP and the LRV. Thus, the EP's and LRV's (center) coordinates were determined by triangulation using stereo frames AS17-134-20422 and AS17-136-20758. Panorama positions are listed in Table 5, and the geolocation of EP-6 is provided by Table 14 (section 3.3).

**Table 4**
*Distances Traveled, Time Ranges, and Approximate Velocities Accomplished on the Traverse Segments Between Stations*

| EVA | from … to … | Travel distance (km) | Travel time[a] (min) | Velocity (km/hr) |
|---|---|---|---|---|
| EVA 1 | LM - sta1 | 1.258 | 13 | 5.8 |
| | sta1 - LM | 1.272 | 14 | 5.4 |
| EVA 2 | LM - sta2 | 8.224 | 73 | 6.8 |
| | sta2 - sta-3 | 3.036 | 41 | 4.4 |
| | sta3 - sta4 | 2.209 | 17 | 7.8 |
| | sta4 - sta5 | 3.247 | 26 | 7.4 |
| | sta5 - LM | 1.431 | 16 | 5.2 |
| EVA 3 | LM - sta6 | 3.476 | 31 | 6.6 |
| | sta6 - sta7 | 0.535 | 7 | 4.6 |
| | sta7 - sta8 | 2.011 | 17 | 7.3 |
| | sta8 - sta9 | 2.082 | 18 | 7.1 |
| | sta9 - LM | 2.423 | 28 | 5.1 |

[a]Apollo 17 Mission Evaluation Team (1973).

#### 3.2.2. EVA 2

On 12 December 1972, the crew explored several craters in the western part of the valley. From the EVA 2 profile (Figure 10) we determined that they traveled 18.147 km in total at an average speed of 6 km/hr (Table 4). Altogether the astronauts spent about 2 hr and 54 min on driving and about the same time at the four major sampling stations (Apollo 17 Mission Evaluation Team, 1973). The highest point reached by the astronauts while on the EVA 2 traverse lies at an elevation of −2,434.3 m and the lowest at −2,628.5 m.

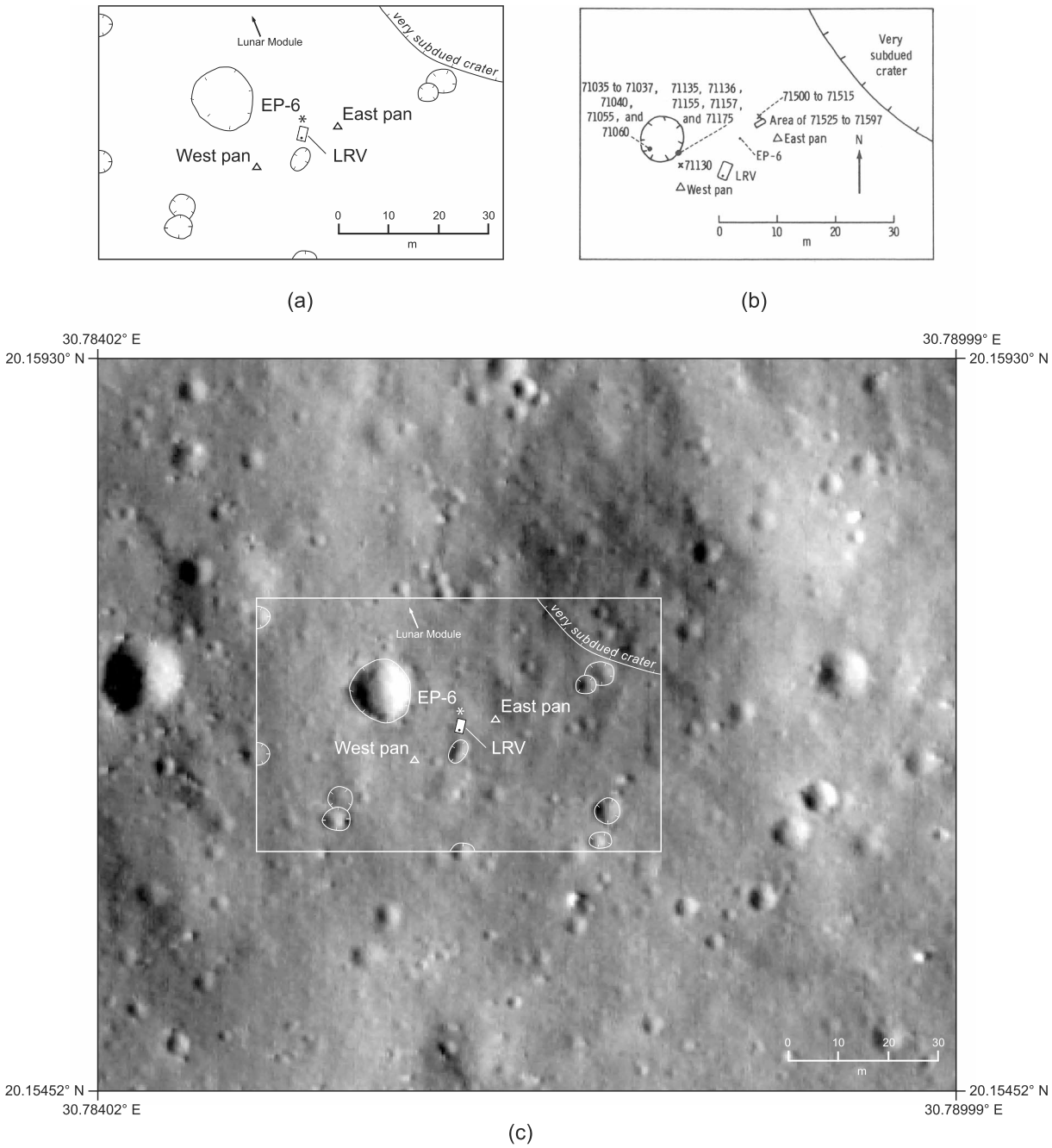


**Figure 9.** Controlled Orthomap of Traverse Station 1. (a) Panorama sites and positions of astronaut equipment were determined by angular network adjustments. (b) Taken from Mühlberger et al. (1973) and is given for comparison and additional information on sample sites. The image base of (c) is Lunar Reconnaissance Orbiter Camera (LROC) Narrow Angle Camera (NAC) image M165645700R (0.4 m/pixel).

**Table 5**
*ME Coordinates in the Region of Traverse Station 1*

| Site | Longitude (°E) | Latitude (°N) | Radius (m) | *X* (m) | *Y* (m) | *Z* (m) |
|---|---|---|---|---|---|---|
| East pan (S/N 1023, color) | 30.78678 | 20.15695 | 1,734,764.1 | 1,399,020.2 | 833,546.0 | 597,787.6 |
| West pan (S/N 1032, b&w) | 30.78622 | 20.15669 | 1,734,764.5 | 1,399,031.1 | 833,533.9 | 597,780.2 |
| LRV | 30.78653 | 20.15690 | 1,734,764.5 | 1,399,024.6 | 833,540.4 | 597,786.3 |

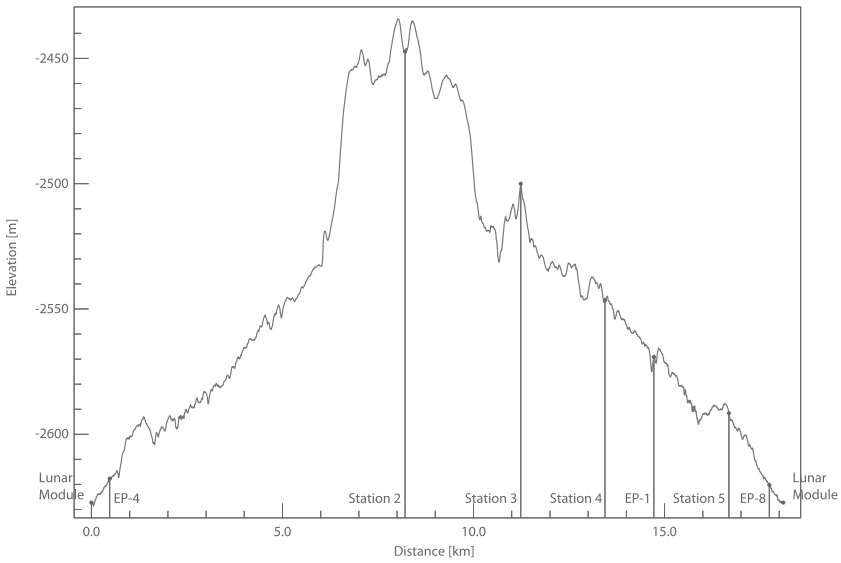


**Figure 10.** Profile of the Lunar Roving Vehicle (LRV) route of EVA 2. The maximum difference in elevation along the astronauts' route is 194.2 m.

The crew's odometer readout at the end of the traverse was 20.2 km (Smith & Mastin, 1973) and is about 2 km longer than the distance derived from the profile (by a factor of 1.11). Reasons for this could be wheel slipping but is more likely related to deviations between the true path and the mapped traverse caused by negotiating boulder fields and small craters as well as rover-pan maneuvers.

#### 3.2.2.1. Station 2

Station 2 is located 7.4 km southwest of the LM, at the foot of the South Massif where it intersects the southeast rim of the Nansen-Apollo depression (see Figure 11). With an elevation of −2,447.3 m it is the highest of all geology stations of the mission and also the most distant point from the LM (7,402 m). The science objectives for the astronauts' tasks of this station were to characterize the South Massif bedrock and the light mantle (a high albedo deposit extending northeast from the South Massif) and to investigate features indicative of the origin of the light mantle (Wolfe et al., 1981). Three boulders from the lower slope of the South Massif were sampled at Station 2. *Boulder 1*, for example, is laying right at the break of slope, and *Boulder 2* rests about 6 m above the valley on the Massif's 14.9 degree slope (26.6%; see Figure 11). In addition to collecting rock and soil samples, the astronauts performed photography and made traverse gravimeter and electrical properties measurements.

Astronaut Cernan recorded a panorama from the lower slope of the South Massif, standing in a small crater located 7 m uphill from the 3-m-wide Boulder 2 (frames AS17-137-20926 to AS17-137-20956). Astronaut Schmitt acquired a panorama at one of the rake sites, at a distance of 29 m and northeast of the LRV (frames AS17-138-21053 to AS17-138-21073). The panoramas are named according to their position relative to the LRV. See Table 6 for corresponding ME coordinates and Figure 12 for a large-scale station map.

#### 3.2.2.2. Station 3

Station 3 is located on the light mantle east of Lara crater, just above the base of the Lee-Lincoln scarp. The science objective at Station 3 was to take a detailed look at the light mantle that covers the scarp in order to determine the interrelations and chronology of the scarp and light mantle materials (Wolfe et al., 1981). Activities at this station included rock and soil sampling, a traverse gravimeter measurement, collection of a double drive tube core, and photography.

At Station 3 only one panorama was taken. From the southern rim of a 12-m-diameter crater astronaut Schmitt acquired frames AS17-138-21150 to 21177. Five single frames of diverse viewing directions were used to determine a mean panorama position given in Table 7. In the exceptional case of frame AS17-138-21168, which is a view to the southeast showing the southern valley and the east Massif in the distance, we could only measure directions to the centers of craters (see Figure 13). This was necessary due to the absence of prominent landmarks, for example, large boulders, to the east of Station 3. However, under

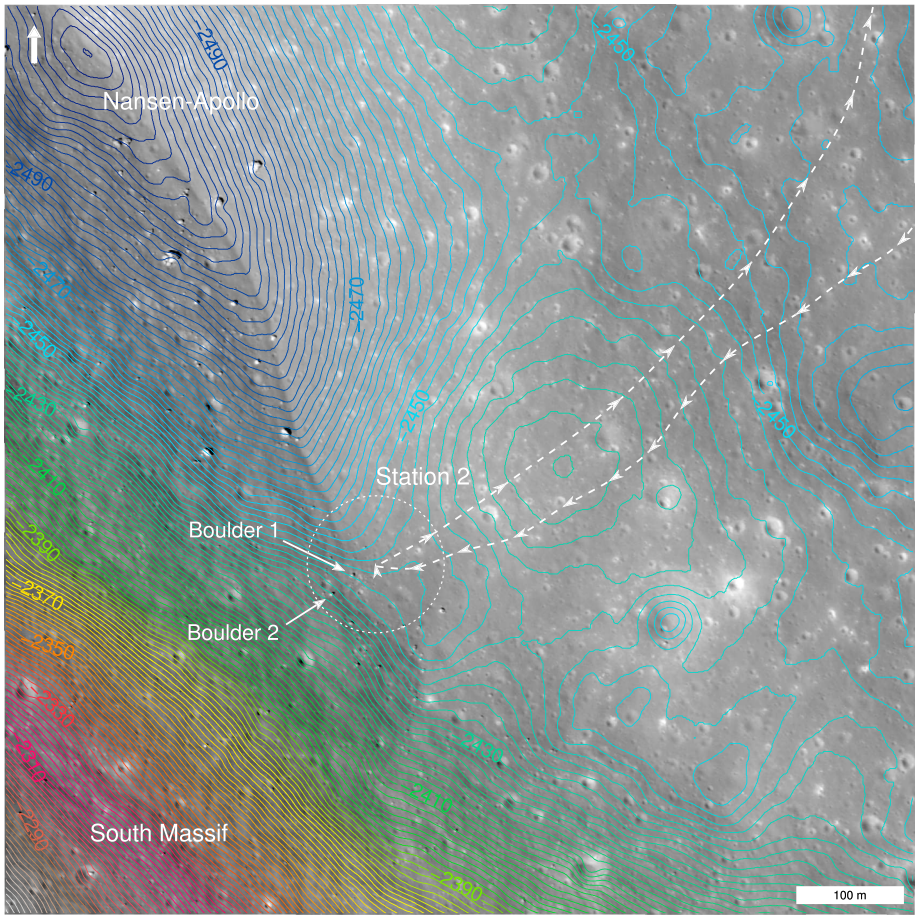


**Figure 11.** Apollo 17's Traverse Station 2 is located to the south of Nansen-Apollo at the base of the northeast slope of the South Massif. The change in elevation between the contour lines is 2 m, and elevation is given relative to a zero vertical datum of the mean lunar radius of 1,737.4 km.

favorable conditions, this proved to be a just as adequate method, provided that a crater's shape or extent is unambiguously discernable in the astronaut image. The deviation of the adjusted camera position of frame AS17-138-21168 to the final, mean panorama site is 1.5 m.

Lacking a second panorama and thus stereo imagery, the position of the LRV was determined by polar point determination making use of the direction and distance from the panorama site. The distance between the perspective center of the camera and the driver's side of the rover, which faces the camera, was estimated to about 12.3 m by using the ratio of the LRV's wheelbase of 2.3 m (Garrett, 1972) as well as its 81-cm wheel diameters, and their respective image sizes in frame AS17-138-21168 (Figure 13a). To determine coordinates of the center of the LRV, we added 1 m to the previously estimated distance to account for the 2-m width of the rover (Garrett, 1972). The parking position of the LRV and the panorama site are mapped in Figure 14, and their coordinates are listed in Table 7.

**Table 6**
*ME Coordinates in the Region of Traverse Station 2*

| Site | Longitude (°E) | Latitude (°N) | Radius (m) | *X* (m) | *Y* (m) | *Z* (m) |
|---|---|---|---|---|---|---|
| SW pan (S/N 1023, color) | 30.52870 | 20.09807 | 1,734,963.7 | 1,403,450.5 | 827,642.7 | 596,182.2 |
| NE pan (S/N 1032, b&w) | 30.53105 | 20.09982 | 1,734,952.4 | 1,403,391.7 | 827,685.7 | 596,228.0 |
| LRV | 30.53033 | 20.09916 | 1,734,952.7 | 1,403,408.3 | 827,671.7 | 596,209.3 |

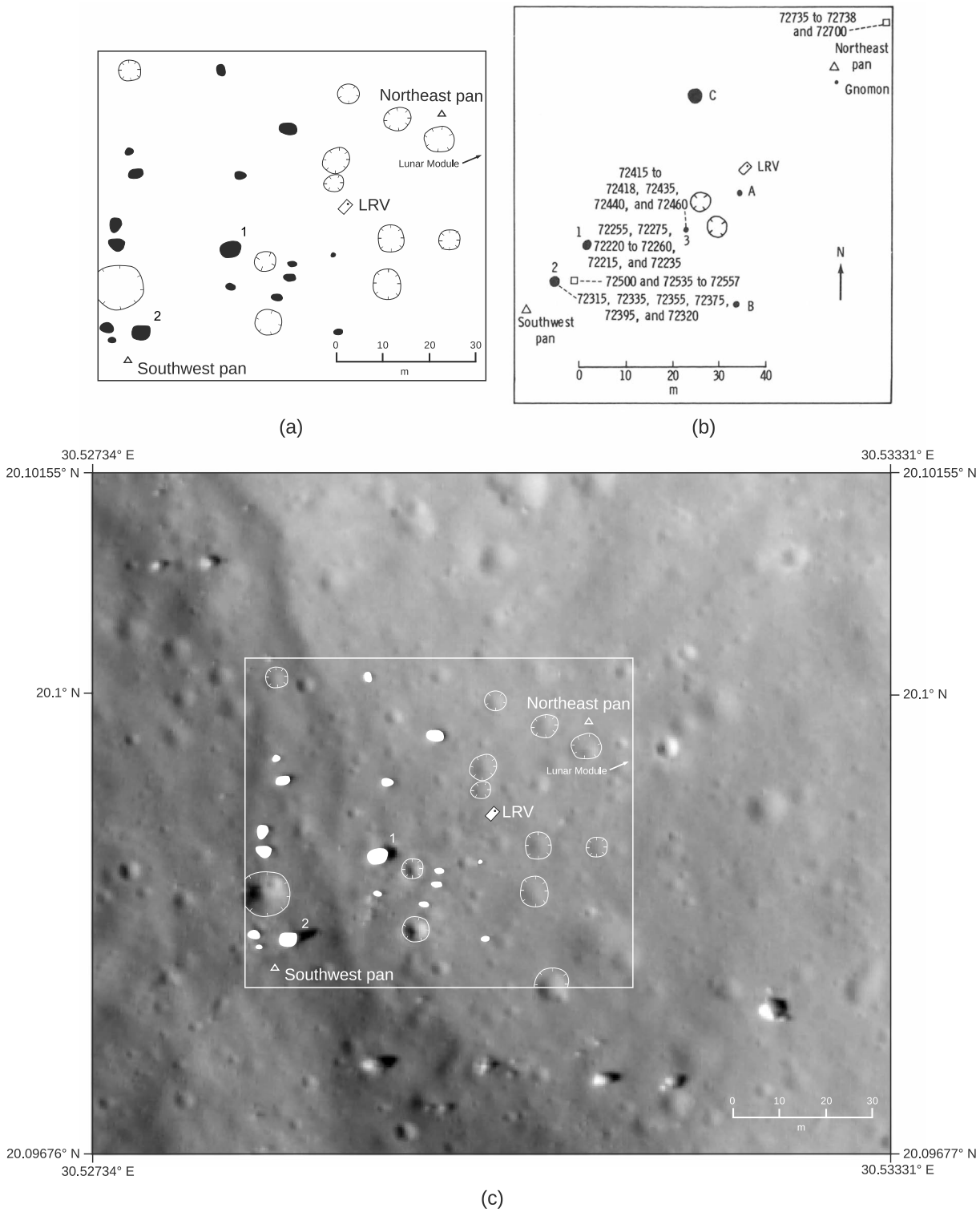


**Figure 12.** Controlled Orthomap of Traverse Station 2. (a) Panorama sites and the Lunar Roving Vehicle (LRV) position were determined by angular network adjustments. (b) Taken from Mühlberger et al. (1973) and is given for comparison and additional information on sample sites. The image base of (c) is Lunar Reconnaissance Orbiter Camera (LROC) Narrow Angle Camera (NAC) image M119652859L (0.4 m/pixel).

**Table 7**
*ME Coordinates in the Region of Traverse Station 3*

| Site | Longitude (°E) | Latitude (°N) | Radius (m) | X (m) | Y (m) | Z (m) |
|---|---|---|---|---|---|---|
| Pan (S/N 1032, b&w) | 30.56512 | 20.17422 | 1,734,902.4 | 1,402,191.0 | 828,101.8 | 598,326.0 |
| LRV | 30.56556 | 20.17402 | 1,734,900.7 | 1,402,185.1 | 828,112.8 | 598,319.8 |

#### 3.2.2.3. Station 4

Station 4 is located on the southern rim crest of Shorty crater, near the northern terminus of the light mantle. Shorty is a 112 m in diameter impact crater, which was originally suspected to be a volcanic vent. The exploration objectives of Station 4 were to examine the crater to determine its origin, sample its surrounding material, and examine the distal end of the light mantle (Wolfe et al., 1981). After the discovery of the unique *orange soil* at the crater rim and because of a shortage of time, observation and sampling were confined to the rim. The crew collected rock and trench samples, a double drive tube core, made traverse gravimeter and electrical properties measurements, and performed photography from the crater rim.

Astronaut Schmitt acquired a panorama standing west of the LRV and close to the large boulder resting on the rim, where he had spotted the orange pyroclastic ash (mapped as sample #74220 in Figure 15b). The frames are AS17-133-20229 to AS17-133-20256. Astronaut Cernan took a color pan standing east of the LRV, moments before they left for their next geology stop. The frames are AS17-137-20991 to AS17-137-21027. The determined astronaut positions are listed in Table 8 and mapped in Figure 15.

#### 3.2.2.4. Station 5

Station 5 is located on the blocky, southwest rim of the large, 608 m in diameter crater Camelot (newly measured crater locations and diameters are provided as supporting information). The exploration objectives of Station 5 were to observe subfloor and dark mantle materials in the floor, rim, and walls of Camelot crater and to sample them on the rim (Wolfe et al., 1981). Activities at this site included a traverse gravimeter measurement, sample collection, and photography.

Astronaut Cernan took a panorama from west of the LRV, standing in the middle of the rim's boulder field. The frames are AS17-145-22159 to AS17-145-22183. Astronaut Schmitt took a second panorama from about 9 m east of the LRV (see Figure 16 and Table 9). The frames are AS17-133-20339 to AS17-133-20360.

### 3.2.3. EVA 3

On 13 December 1972, the astronauts' third and last excursion went northward to the base of the North Massif, the Sculptured Hills, and Van Serg crater. A profile of the astronauts' traverse path of EVA 3 is given in Figure 17. We determined the lengths of the driven route sections between the four major sample stations adding up to 10.527 km in total (Table 4). The highest point of the EVA 3 traverse lies at an elevation of

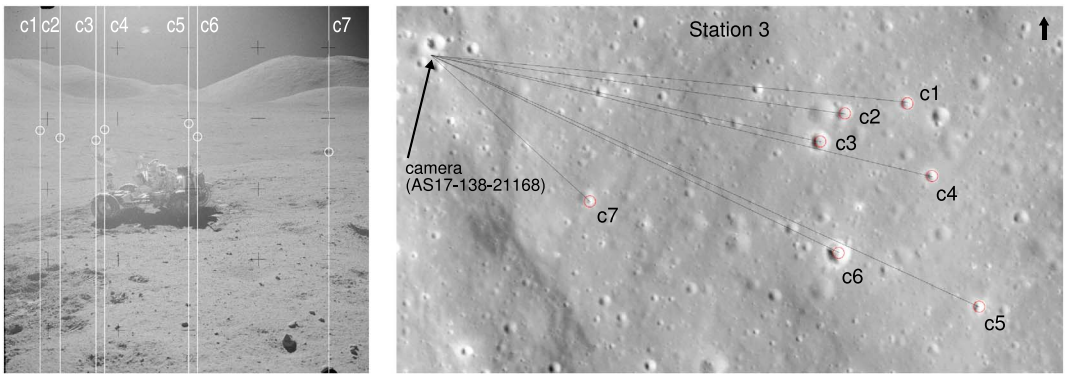


(a) (b)

**Figure 13.** (a) Due to the absence of prominent surface features southeast of Station 3, for example, large boulders, here only centers of craters (c1–c7) were used for camera positioning (AS17-138-21168). (b) After identification of the same craters in the Lunar Reconnaissance Orbiter Camera (LROC) Narrow Angle Camera (NAC) orthomosaic, the network of directions was adjusted to the center coordinates of the craters. The distances between the astronaut/camera and the craters range from 153 m (c7) to 429 m (c5).

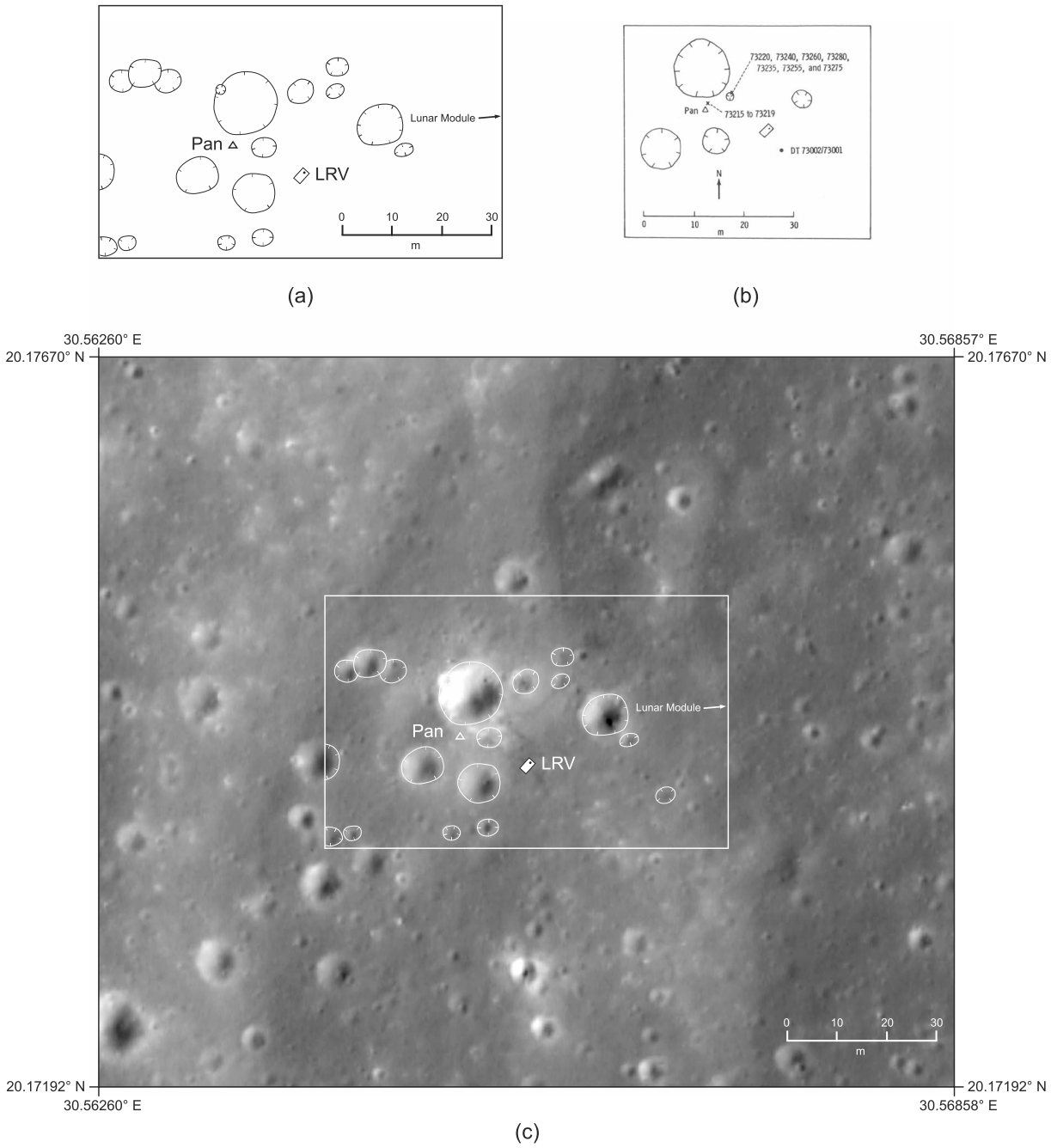


**Figure 14.** Controlled orthomap of Traverse Station 3. (a) The panorama site and the Lunar Roving Vehicle (LRV) position were determined by angular network adjustments. (b) Taken from Mühlberger et al. (1973) and is given for comparison and additional information on sample sites. The image base of (c) is Lunar Reconnaissance Orbiter Camera (LROC) Narrow Angle Camera (NAC) image M175077349R (0.2 m/pixel).

−2,563.8 m and the lowest at −2,667.5 m. The crew spent 1 hr and 41 min on driving (including minor sample stops and charge deployment) and 3 hr and 21 min on field work at the geology stops (Apollo 17 Mission Evaluation Team, 1973). We determined the velocity along the EVA 3 traverse to about 6 km/hr on average. Similar to EVA 2, the odometer distance at the end of the traverse (12.0 km) provided by Smith and Mastin (1973) is longer than the mapped traverse by a factor of 1.14.

#### 3.2.3.1. Station 6

Station 6 is located on the south slope of the North Massif, 410 m northeast of so-called *Turning Point Rock* and to the north of Henry crater. The area is on a 15.4 degree slope (27.6%) and covered with large

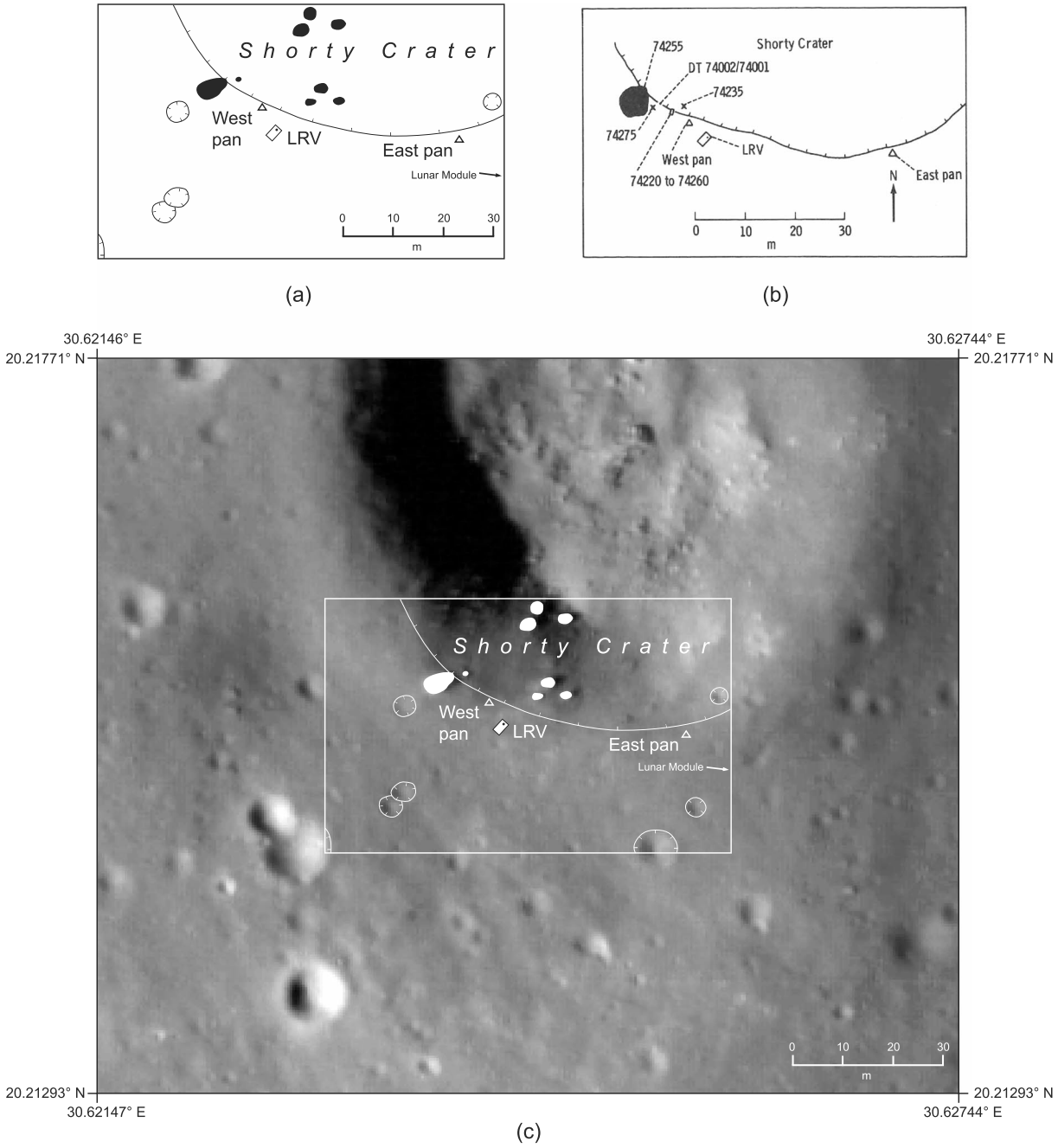


**Figure 15.** Controlled orthomap of Traverse Station 4. (a) Panorama sites and the Lunar Roving Vehicle (LRV) position were determined by angular network adjustments. (b) Taken from Mühlberger et al. (1973) and is given for comparison and additional information on sample sites. The image base of (c) is Lunar Reconnaissance Orbiter Camera (LROC) Narrow Angle Camera (NAC) image M119652859R (0.4 m/pixel).

**Table 8**
*ME Coordinates in the Region of Traverse Station 4*

| Site | Longitude (°E) ) | Latitude (°N) | Radius (m) | *X* (m) | *Y* (m) | *Z* (m) |
|---|---|---|---|---|---|---|
| West pan (S/N 1032, b&w) | 30.62418 | 20.21548 | 1,734,853.5 | 1,400,926.1 | 829,303.6 | 599,481.7 |
| East pan (S/N 1023, color) | 30.62555 | 20.21527 | 1,734,853.8 | 1,400,908.4 | 829,338.4 | 599,475.7 |
| LRV | 30.62427 | 20.21532 | 1,734,854.0 | 1,400,926.7 | 829,306.9 | 599,477.2 |

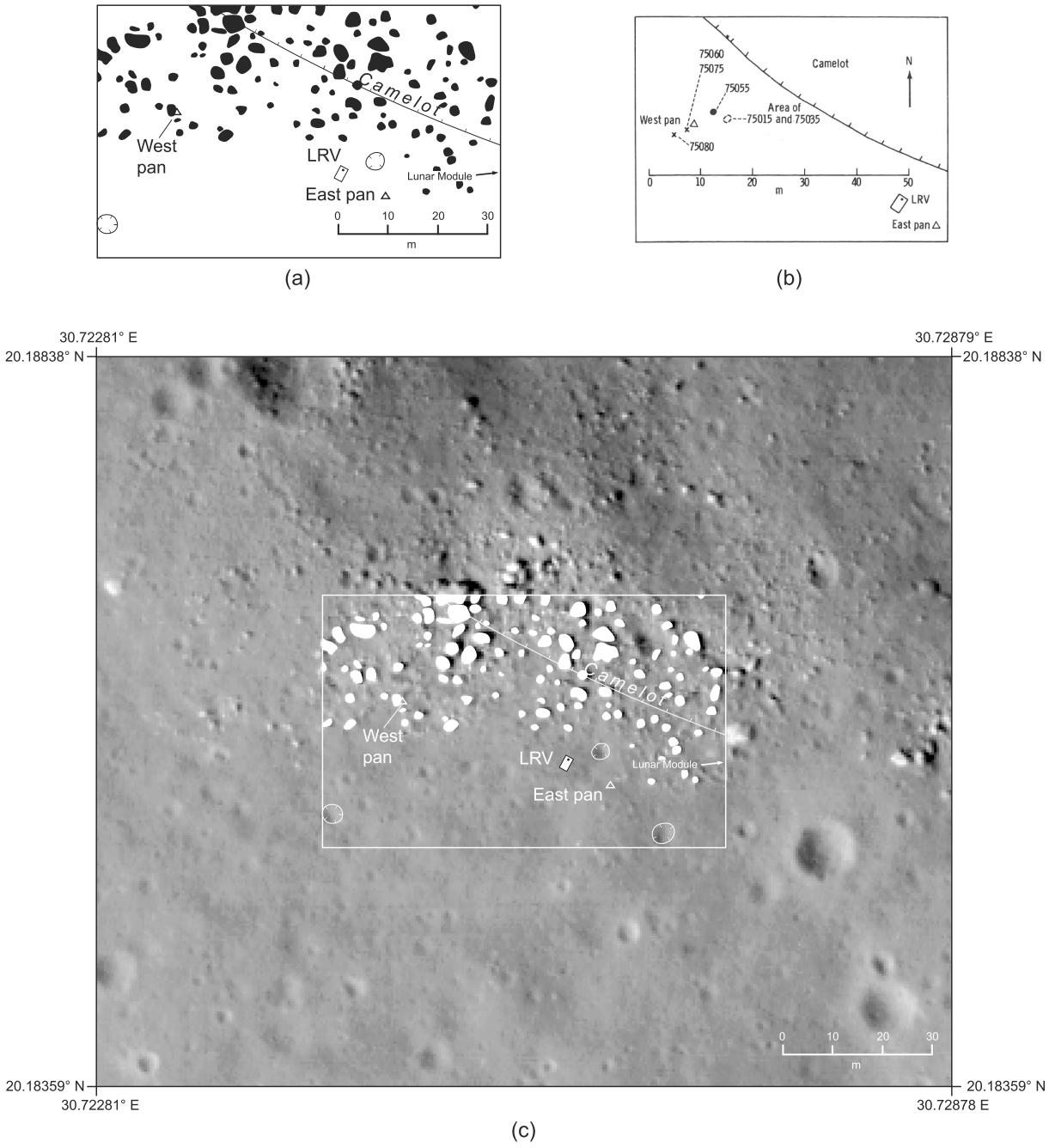


**Figure 16.** Controlled orthomap of Traverse Station 5. (a) Panorama sites and the Lunar Roving Vehicle (LRV) position were determined by angular network adjustments. (b) Taken from Mühlberger et al. (1973) and is given for comparison and additional information on sample sites. The image base of (c) is Lunar Reconnaissance Orbiter Camera (LROC) Narrow Angle Camera (NAC) image M168000580 L (0.25 m/pixel).

**Table 9**
*ME Coordinates in the Region of Traverse Station 5*

| Site | Longitude (°E) | Latitude (°N) | Radius (m) | *X* (m) | *Y* (m) | *Z* (m) |
|---|---|---|---|---|---|---|
| West pan (S/N 1023, color) | 30.72495 | 20.18613 | 1,734,810.9 | 1,399,694.8 | 831,902.6 | 598,632.9 |
| East pan (S/N 1032, b&w) | 30.72641 | 20.18557 | 1,734,808.3 | 1,399,676.6 | 831,940.0 | 598,616.0 |
| LRV | 30.72611 | 20.18572 | 1,734,808.9 | 1,399,680.1 | 831,932.2 | 598,620.5 |

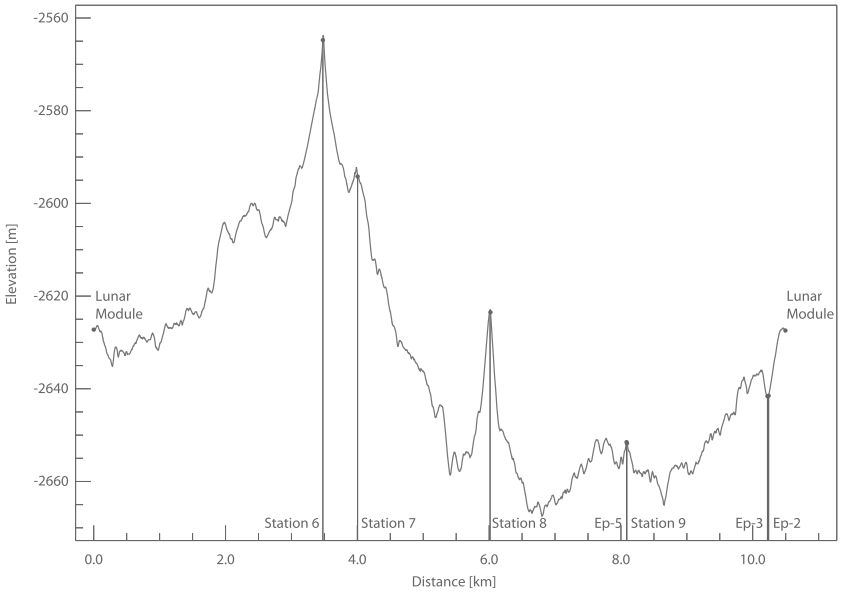


**Figure 17.** Profile of the EVA 3 traverse path. The maximum difference in elevation along the astronauts' route is 103.7 m.

boulders, which had rolled down from higher on the massif leaving behind prominent tracks (see Figure 18). The crew drove cross slope up to a massive, split boulder located about 30 m above the valley floor and parked side-on 15 m west of it (see Figure 19 and Table 10). The boulder had rolled down a 22.5 degree slope (41.4%) forming a 10-m-wide trail that begins 394 m above and ends after 1,030 m at the boulder's present location where it had broken apart into five major pieces. The exploration objectives of Station 6 were to characterize and sample the blocks and sediment of the North Massif and dark mantle materials that locally cover the region (Wolfe et al., 1981). Activities at this site included sample collection, collection of a single drive tube core, a traverse gravimeter measurement, and photography.

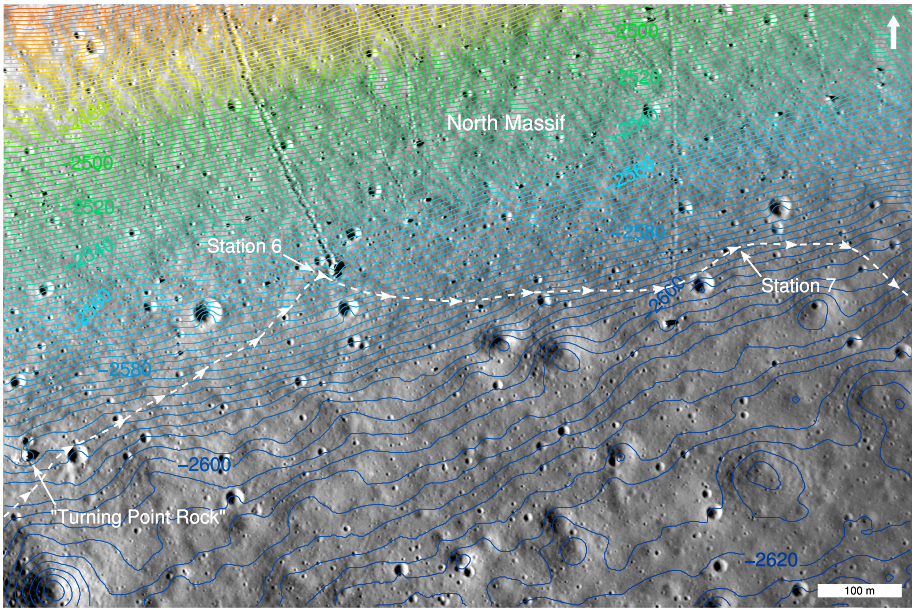


**Figure 18.** Apollo 17's two northernmost traverse stations on the south slope of the North Massif. The traverse path of the crew, represented as a dashed line, is based on the Traverse Map from the Apollo era (Defense Mapping Agency, 1975) and illustrates an estimate only. The change in elevation between the contour lines is 2 m, and elevation is given relative to a mean lunar radius of 1,737.4 km.

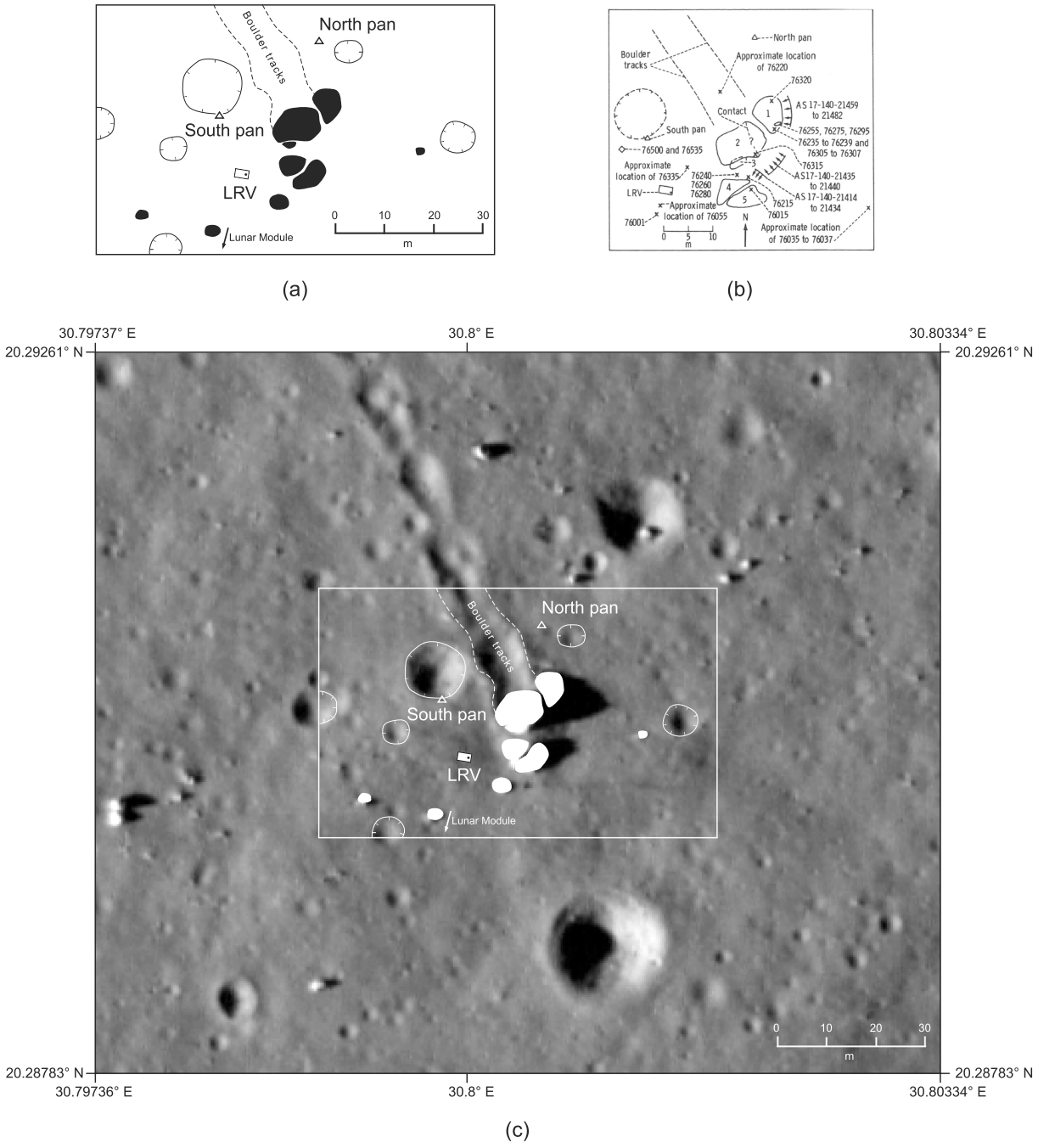


**Figure 19.** Controlled orthomap of Traverse Station 6. (a) Panorama sites and the Lunar Roving Vehicle (LRV) position were determined by angular network adjustments. (b) Taken from Mühlberger et al. (1973) and is given for comparison and additional information on sample sites. The image base of (c) is Lunar Reconnaissance Orbiter Camera (LROC) Narrow Angle Camera (NAC) image M165645700R (0.4 m/pixel).

**Table 10**
*ME Coordinates in the Region of Traverse Station 6*

| Site | Longitude (°E) | Latitude (°N) | Radius (m) | *X* (m) | *Y* (m) | *Z* (m) |
|---|---|---|---|---|---|---|
| South pan (S/N 1032, b&w) | 30.79981 | 20.29031 | 1,734,838.3 | 1,397,691.5 | 833,185.1 | 601,602.0 |
| North pan (S/N 1023, color) | 30.80051 | 20.29080 | 1,734,840.6 | 1,397,678.7 | 833,200.7 | 601,616.8 |
| LRV | 30.79997 | 20.28993 | 1,734,835.4 | 1,397,690.3 | 833,189.6 | 601,590.2 |

Astronaut Schmitt found level ground on the southern rim of a small crater, 11 m in diameter, from where he acquired the *South Pan*. The frames are AS17-141-21575 to AS17-141-21603, and the standard deviation of the determined panorama position is ±0.8 m. Astronaut Cernan recorded a panorama north of the boulder on the east side of the boulder tracks, leveling himself by standing in a little hole. The frames are AS17-140-21483 to AS17-140-21509, and the standard deviation of the mean panorama position is ±0.5 m.

#### 3.2.3.2. Station 7

Station 7 is located 490 m east of Station 6, on the lower slope of the North Massif just above the break in slope between the Massif and the valley floor (Figure 18). The area is located on a 13.6 degree slope (24.2%) and covered with boulders, which had rolled down from higher on the Massif. The exploration objectives for Station 7 were the same as for Station 6, which were to characterize and sample Massif and dark mantle materials (Wolfe et al., 1981). The crew gathered samples and performed photography at this site.

Astronaut Schmitt recorded a panorama south of the rover at 11-foot focus and aiming the camera low to document the near-field sampling area. The frames, showing almost none of the horizon, are AS17-141-21646 to AS17-141-21664, and the standard deviation of the mean panorama position is ±0.7 m. Astronaut Cernan took a standard 74-foot panorama for *location work*, as he puts it, standing in a small crater north of the rover, which provided him a somewhat level ground. See the large-scale station map in Figure 20 and Table 11 for station coordinates. The frames are AS17-146-22339 to AS17-146-22363, and the standard deviation of the mean panorama position is ±0.8 m.

#### 3.2.3.3. Station 8

Station 8 is located 3,972 m northeast of the LM near the base of the Sculptured Hills on a southwest facing slope just southeast of Wessex Cleft. The exploration objectives were to sample Sculptured Hills material. From northeast of Bowen-Apollo (referred to as *SWP* during the course of the mission) the crew drove about 110 m up slope (20.6%) and parked the LRV about 22 m above the valley floor on the northeastern rim of a small, 10-m crater (see Figure 21). Activities at this site included two traverse gravimeter measurements, sample collection including trench samples, and photography.

Astronaut Cernan acquired a panorama 55 m upslope and east of the LRV (see Figure 22) near the boulder he and astronaut Schmitt had sampled and pushed downhill. The frames are AS17-146-22375 to AS17-146-22397. Astronaut Schmitt recorded a second pan close to the trench site (see sample sequence 78420-78480 in Figure 22b) just before they left for the next station. The frames are AS17-142-21726 to AS17-142-21745. The slope of Station 8 made it difficult for the astronauts to level themselves during image acquisition. Also, Station 8 lacks prominent surface features in the vicinity to use as network control as the largest rock the crew had seen at Station 8 was less than 1 m in size (Wolfe et al., 1981). Therefore, our calculations relied mainly on measurements to far-distant features located in the south and west at distances ranging from 500 m (rocks on the southern rim of Bowen-Apollo) to as far as 2.6 km (large boulders at the base and lower slope of the North Massif). Hence, mean panorama positions had relatively high (lateral) standard deviations of 1.4 and 4.0 m for the East and the West Pan, respectively. Our results are listed in Table 12.

#### 3.2.3.4. Station 9

The final traverse stop, Station 9, is located on the southeast rim and blocky ejecta blanket of Van Serg crater. It is a young impact crater, 106 m in diameter, and was chosen in order to study more recent cratering events. The exploration objectives were to determine the crater's origin (originally suspected to be volcanic) and to sample the dark mantle and its subfloor material (Wolfe et al., 1981). Activities at this site included collection of a double drive tube sample, traverse gravimeter measurements, sample collection including trench samples, charge deployment, and photography.

Astronaut Schmitt acquired a first panorama at the location labeled West Pan in Figure 23. The frames are AS17-142-21798 to AS17-142-21824. At the same time astronaut Cernan took a (partial) panorama at the location labeled *North Pan*, achieving only about three fourths of a full turn, because he ran out of film. The frames are AS17-146-22423 to AS17-146-22450. Astronaut Schmitt acquired a second panorama at the location labeled South Pan, capturing the emplaced seismic charge (EP-5) as well as astronaut Cernan obtaining a core sample in the white material they found near the LRV. The frames are AS17-142-21836 to AS17-142-21858. The determined geolocations are mapped in Figure 23, and the corresponding coordinates are listed in Table 13.

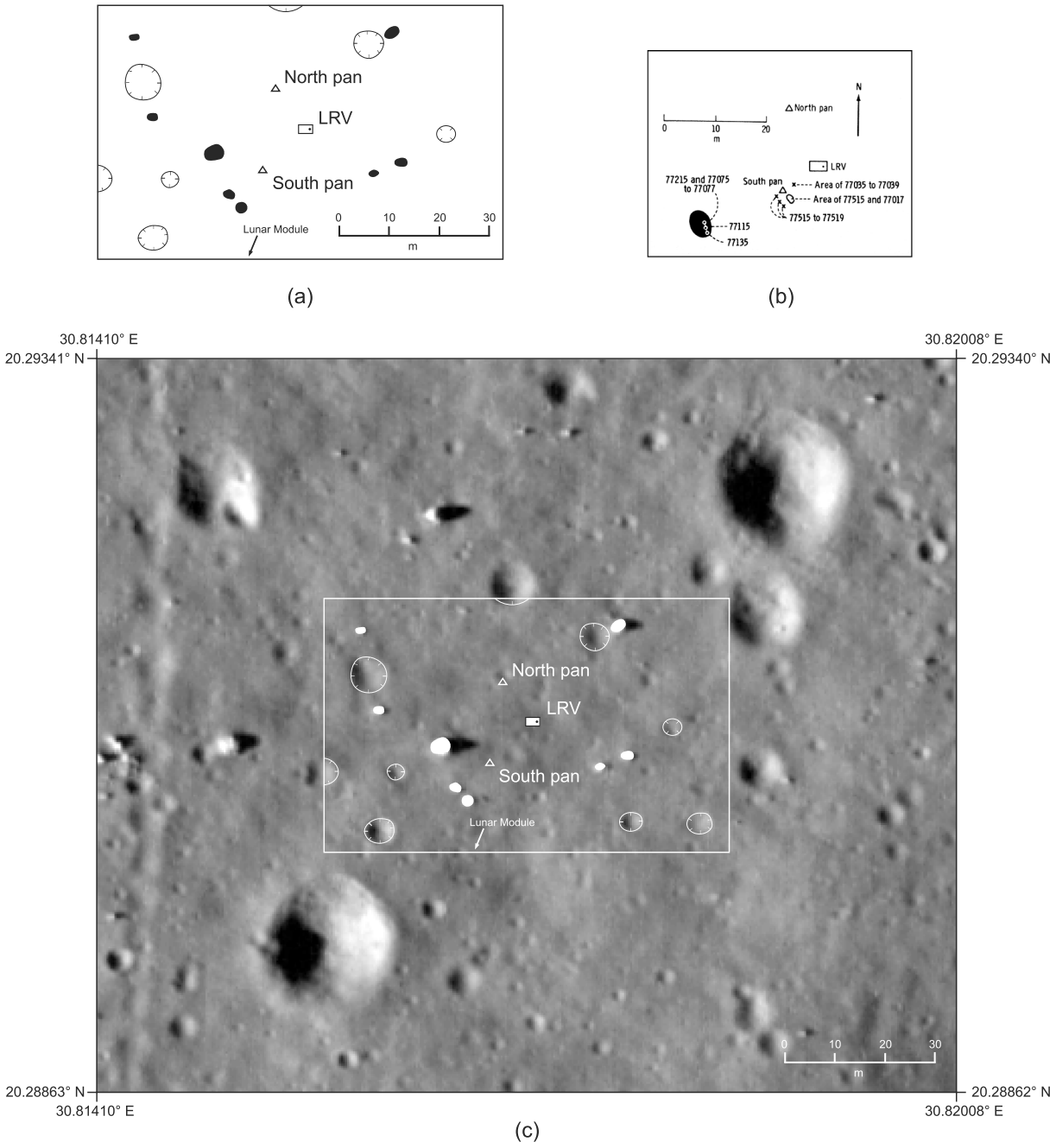


**Figure 20.** Controlled orthomap of Station 7. (a) Panorama sites and the Lunar Roving Vehicle (LRV) position were determined by angular network adjustments. (b) Taken from Mühlberger et al. (1973) and is given for comparison and additional information on sample sites. The image base of (c) is Lunar Reconnaissance Orbiter Camera (LROC) Narrow Angle Camera (NAC) image M165645700R (0.4 m/pixel).

**Table 11**
*ME Coordinates in the Region of Traverse Station 7*

| Site | Longitude (°E) | Latitude (°N) | Radius (m) | *X* (m) | *Y* (m) | *Z* (m) |
|---|---|---|---|---|---|---|
| South pan (S/N 1032, b&w) | 30.81684 | 20.29078 | 1,734,805.6 | 1,397,413.3 | 833,582.2 | 601,604.0 |
| North pan (S/N 1023, color) | 30.81692 | 20.29130 | 1,734,809.1 | 1,397,410.1 | 833,583.2 | 601,620.2 |
| LRV | 30.81714 | 20.29104 | 1,734,806.8 | 1,397,407.5 | 833,588.6 | 601,611.9 |

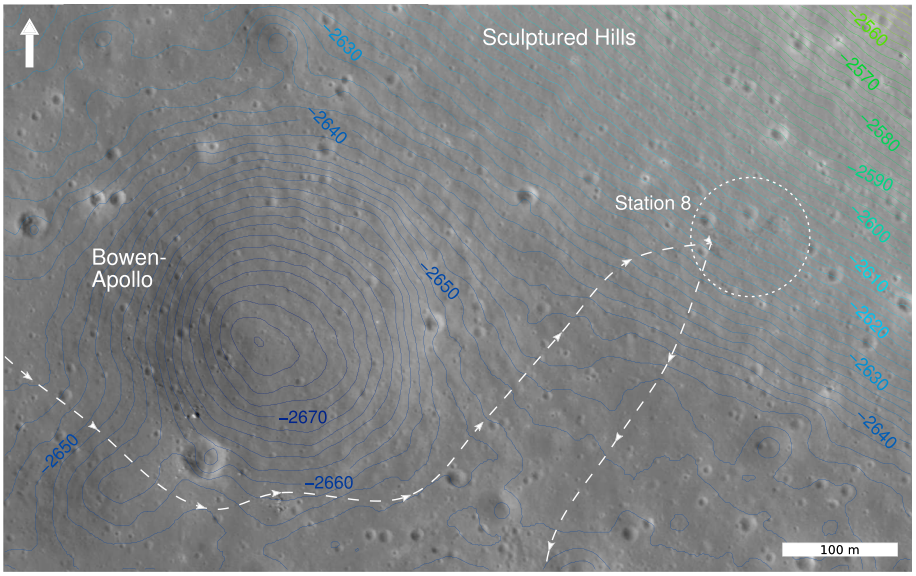


**Figure 21.** Apollo 17's easternmost geology stop on the base of the southwest slope of Sculptured Hills. The traverse path of the crew, represented as a dashed line, is based on the Traverse Map from Apollo times (Defense Mapping Agency, 1975) and illustrates an estimate only. The change in elevation between the contour lines is 2 m, and elevation is given relative to a mean lunar radius of 1,737.4 km.

### 3.3. Coordinates of the LSPE Seismic Sources

At eight designated sites in the Taurus-Littrow Valley the astronauts deployed Explosive Packages (EPs) containing from 57 to 2,722 g of high explosives. EPs and the geophones constitute the *Apollo 17 Geophysical Station* (Kovach et al., 1973). To this day, Apollo 17's LSPE is the largest active seismic experiment, which was ever set up on the lunar surface to determine the internal, near-surface structure (see Figure 24 for the EP deployment sites).

The astronauts deployed the EPs either en route by setting them down on the ground without getting off the LRV (EP-1, EP-4, EP-7, and EP-8) or during preplanned geology stops of longer duration. Figure 25a shows astronaut Schmitt during Apollo 17 preflight training as he deploys an EP from the passenger's seat of the rover mock-up. Subsequently, the crew acquired either *locator* images with the charges imaged in the foreground and the LM in the background (Figure 25b) or so-called *rover* or *LRV pans* for documentation and positioning purposes.

The rover-pan technique, where astronaut Schmitt would take a sequence of panoramic images from the passenger's seat while astronaut Cernan slowly steered around the emplaced charge in a tight, clockwise circle, was used for EP-1, EP-4, and EP-7. The charge constitutes the (approximate) center of the driven circle and was not imaged itself. To localize the deployment site of an explosive charge, we determined locations of the camera's perspective center of several frames on the approximate rover-pan circle. The center of the circle was assumed to be the EP position. While the minimum technically possible turning radius of the LRV is given to be 3.1 m (Costes et al., 1972), we estimate radii of the LRV-turns around the charges of approximately 4–6 m. EP positions derived in this manner have a relatively high uncertainty of approximately up to ±3 m, depending on the derived radius of the respective rover-pan.

EP-6, which was deployed at Station 1 during EVA 1, is the only charge captured within a stereo image pair (frames AS17-136-20758 and AS17-134-20422), both frames being members of the panoramas routinely taken at each station. Here the positional accuracy is relatively high, amounting to ±0.5 m. In most cases, whenever locator images were available, the respective EP position was determined by applying the geodetic method called polar point determination. For example, even though EP-8 was deployed en route, it was captured in a locator image (Figure 25b). Once the frame's position and azimuth (to north) were determined, we derived the direction angle and the distance to the seismic charge, which needed to be imaged in its full dimension. Assuming nearly vertical alignment of the EP's receiving antenna and the image plane as well

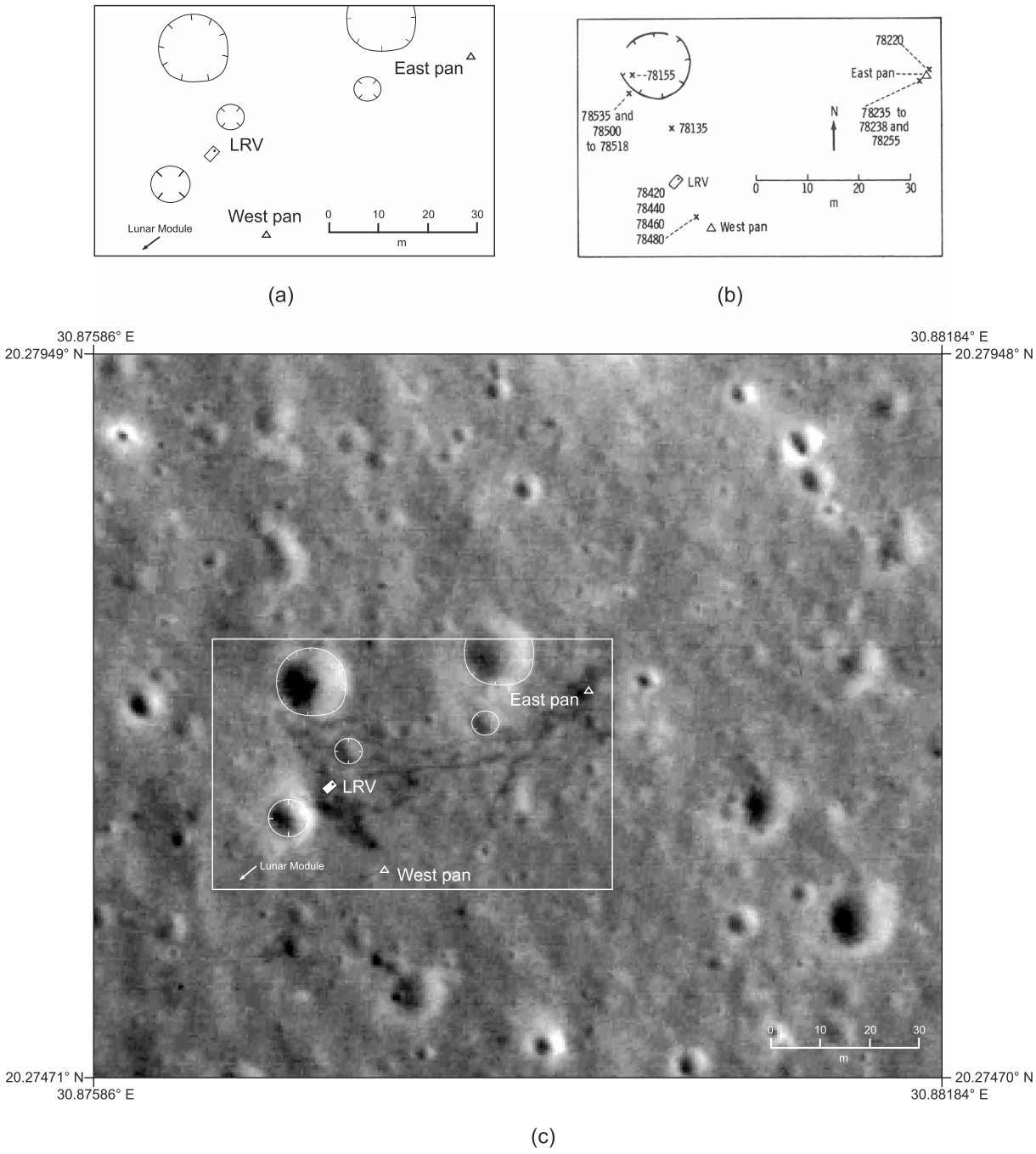


**Figure 22.** Controlled orthomap of Traverse Station 8. (a) Panorama sites and the Lunar Roving Vehicle (LRV) position were determined by angular network adjustments. (b) Taken from Mühlberger et al. (1973) and is given for comparison and provides an overview on sample sites. The image base of (c) is Lunar Reconnaissance Orbiter Camera (LROC) Narrow Angle Camera (NAC) image M152669024L (0.4 m/pixel).

**Table 12**
*ME-Coordinates in the Region of Traverse Station 8*

| Site | Longitude (°E) | Latitude (°N) | Radius (m) | *X* (m) | *Y* (m) | *Z* (m) |
|---|---|---|---|---|---|---|
| East pan (S/N 1023, color) | 30.87936 | 20.27727 | 1,734,788.4 | 1,396,610.7 | 835,171.0 | 601,214.4 |
| West pan (S/N 1032, b&w) | 30.87791 | 20.27608 | 1,734,775.2 | 1,396,631.8 | 835,135.8 | 601,176.2 |
| LRV | 30.87753 | 20.27663 | 1,734,777.3 | 1,396,634.2 | 835,124.5 | 601,192.4 |

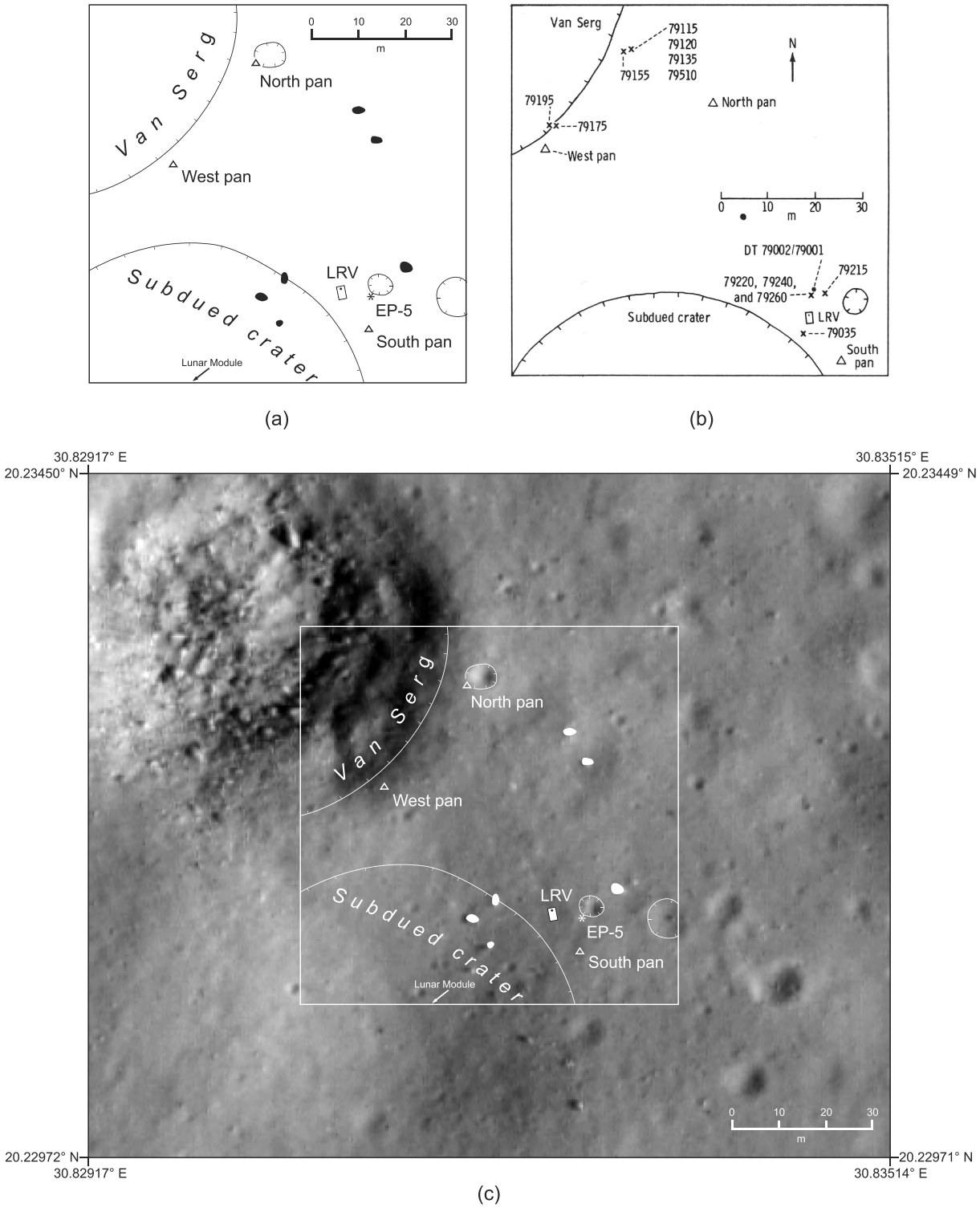


**Figure 23.** Controlled orthomap of Traverse Station 9. (a) Panorama sites and the Lunar Roving Vehicle (LRV) position were determined by angular network adjustments. (b) Taken from Mühlberger et al. (1973) and is given for comparison and additional information on sample sites. The image base of (c) is Lunar Reconnaissance Orbiter Camera (LROC) Narrow Angle Camera (NAC) image M129086118L (0.4 m/pixel).

**Table 13**
*ME Coordinates in the Region of Traverse Station 9*

| Site | Longitude (°E) | Latitude (°N) | Radius (m) | *X* (m) | *Y* (m) | *Z* (m) |
|---|---|---|---|---|---|---|
| West pan (S/N 1032, b&w) | 30.83138 | 20.23231 | 1,734,751.9 | 1,397,684.8 | 834,225.1 | 599,924.8 |
| North pan (S/N 1023, color) | 30.83199 | 20.23302 | 1,734,751.8 | 1,397,669.4 | 834,236.3 | 599,944.9 |
| South pan (S/N 1032, b&w) | 30.83284 | 20.23116 | 1,734,747.7 | 1,397,670.6 | 834,264.9 | 599,890.5 |
| LRV | 30.83264 | 20.23141 | 1,734,748.7 | 1,397,672.0 | 834,259.3 | 599,897.9 |

as knowing the length of the fully extended antenna, that is, 1.65 m (Lauderdale & Eichelman, 1974), we approximated the distance between the optical center of the Hasselblad camera and the charge by using elevation angles measured in the locator image. In the case of Figure 25b we determined the distance between EP-8 and the optical center of the Hasselblad camera to about 6.5 m. Table 14 lists the determined ME coordinates of the eight charges in spherical and Cartesian coordinates. Radii were derived from the LROC NAC DTM.

Geolocations of the four charges deployed close to the LM site are mapped in Figure 26. The two EPs deployed during geology stops, that is, EP-6 and EP-5, are mapped in the corresponding large-scale maps of Station 1 (Figure 9) and Station 9 (Figure 23). Large-scale maps of EP-7 (deployed on the way back from Station 1) and EP-1 (Victory Crater; see Figure 4 in section 2.3) are not available, but their geolocations are mapped in Figure 24.

### 3.3.1. Improved LSPE Source-Receiver Distances

The deployed EPs were remotely detonated one after the other, a few hours after the crew had departed. Seismic waves induced by these detonations were recorded by the four-geophone array located near the center of the valley (see Figure 26) and telemetered back to Earth along with timing data (Apollo 17 Mission Evaluation Team, 1973). The thrust of the LM ascent engines, the subsequent impact of the LM ascent stage on the adjacent highlands (the impact location of the LM ascent stage could not be identified in LROC images yet), and also natural seismic events were recorded, and the historic recordings are made available by the National Space Science Data Center (NSSDC). Recently, the Apollo 17 seismic data were closely reviewed by different geophysicists groups (Heffels et al., 2017; Sollberger et al., 2016). Besides accurate shot times the knowledge of accurate ranges between source and receiver is fundamental in the analysis of the geophone data. To support ongoing reanalysis, we provide a complete list of improved source-receiver distances derived from the newly determined LSPE positions (see Table A5 in Appendix A).

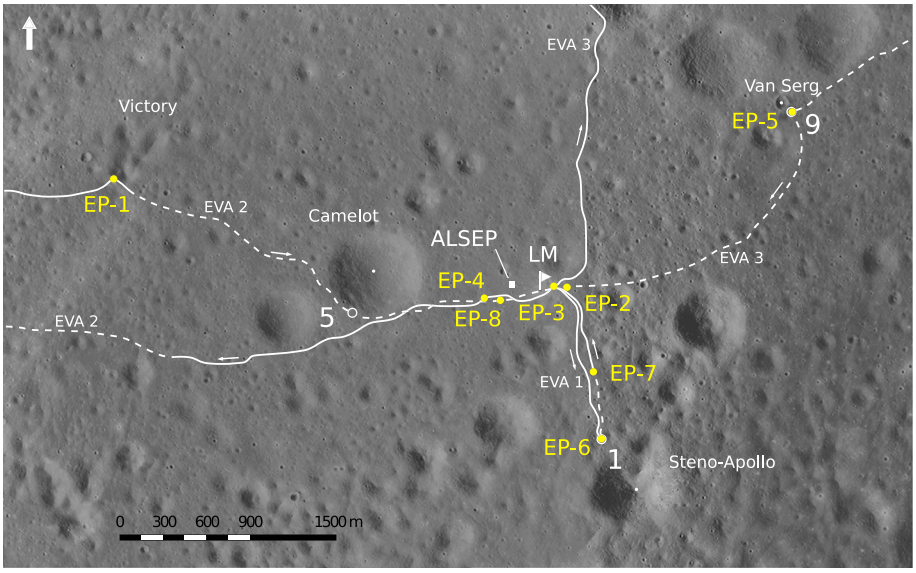


**Figure 24.** Geolocations of the Explosive Packages of the active seismic sounding experiment Lunar Seismic Profiling Experiment (LSPE). The charges were remotely detonated after the Apollo 17 crew had left the lunar surface.

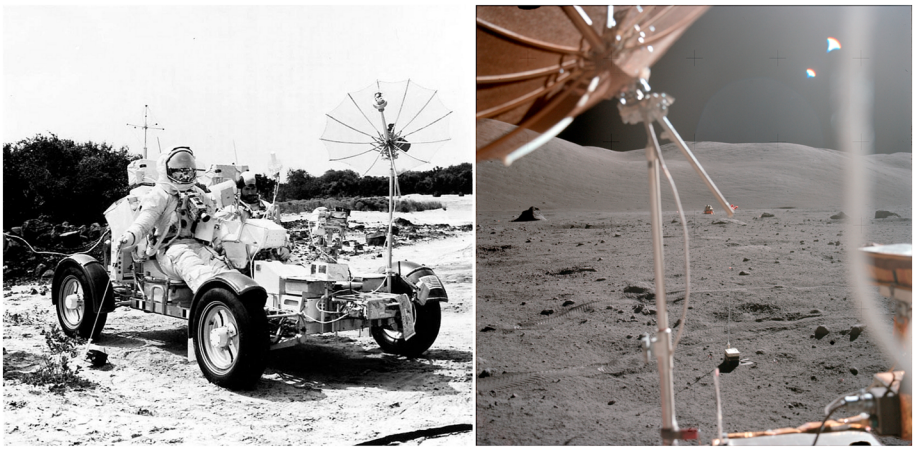

(a) (b)

**Figure 25.** (a) Practicing deployment of explosive charges during EVA training at Sunset Crater, Flagstaff, Arizona (NASA Photo 72-H-1411, source: Apollo Lunar Surface Journal [ALSJ]). (b) Locator image to the Lunar Module (LM; image center) acquired from the driver's seat by E. Cernan. Seismic charge EP-8 is displayed in the foreground and Geophone Rock is to the left (AS17-145-22184).

### 3.4. New Apollo 17 Landing Site Map (1:15000)

The DTM, the orthomosaic, and the feature positions determined in this study were combined to create a new map of the Apollo 17 landing site (Figure 27). Its map-sheet designation is L15K 20.2/30.7East COMT. *L* stands for Moon, *15K* specifies the map's scale of 1:15000, *20.2/30.7 East* designates the planetocentric latitude and longitude to the nearest decimal degree nearest to the center point of the map, and *COMT* is an acronym for *Controlled Orthophoto Mosaic with Topography*.

The map covers an area of about 14 km × 12 km of the Taurus-Littrow Valley, from 30.4294° to 30.9162° in longitude and from 19.9771° to 20.3639° in latitude. Planetocentric coordinates given in the map are related to the ME lunar reference system, according to LRO project standards and as recommended by the International Astronomical Union/International Association of Geodesy (IAU/IAG) Working Group on Cartographic Coordinates and Rotational Elements. The map includes a graticule, contour lines with an equidistance of 50 m, the astronauts' traverses, and their major geology stops. IAU-approved as well as non-IAU-approved, but commonly used feature names, for example, craters, massifs, and mountains, are labeled. Center coordinates and diameters of named craters were remeasured for mapping purposes and for the provision of supporting information.

The LRV parking positions at the traverse stations whose coordinates were determined within this study were chosen to define the respective station locations in the traverse map, and hence, constitute the center of the mapped red circles representing the geology stations. The astronauts' paths between them were reconstructed by referencing and adopting the NASA Apollo 17 Traverse Map (Defense Mapping Agency, 1975)

**Table 14**
*ME Coordinates of the Apollo 17 Explosive Packages*

| Charge | EVA | Longitude (°E) | Latitude (°N) | Radius (m) | *X* (m) | *Y* (m) | *Z* (m) |
|---|---|---|---|---|---|---|---|
| EP-6 | 1 | 30.78653 | 20.15700 | 1,734,764.5 | 1,399,023.7 | 833,539.9 | 597,789.1 |
| EP-7 | 1 | 30.78458 | 20.17226 | 1,734,765.4 | 1,398,916.0 | 833,411.2 | 598,223.0 |
| EP-4 | 2 | 30.75813 | 20.18904 | 1,734,782.8 | 1,399,164.0 | 832,684.0 | 598,705.9 |
| EP-1 | 2 | 30.66821 | 20.21618 | 1,734,832.6 | 1,400,265.2 | 830,366.2 | 599,494.4 |
| EP-8 | 2 | 30.76202 | 20.18854 | 1,734,779.7 | 1,399,109.4 | 832,780.1 | 598,690.8 |
| EP-5 | 3 | 30.83285 | 20.23139 | 1,734,748.2 | 1,397,668.6 | 834,264.3 | 599,897.3 |
| EP-2 | 3 | 30.77820 | 20.19150 | 1,734,772.2 | 1,398,841.6 | 833,155.8 | 598,772.1 |
| EP-3 | 3 | 30.77500 | 20.19175 | 1,734,773.0 | 1,398,886.5 | 833,076.8 | 598,779.6 |

*Note*. Listed in the order of deployment.

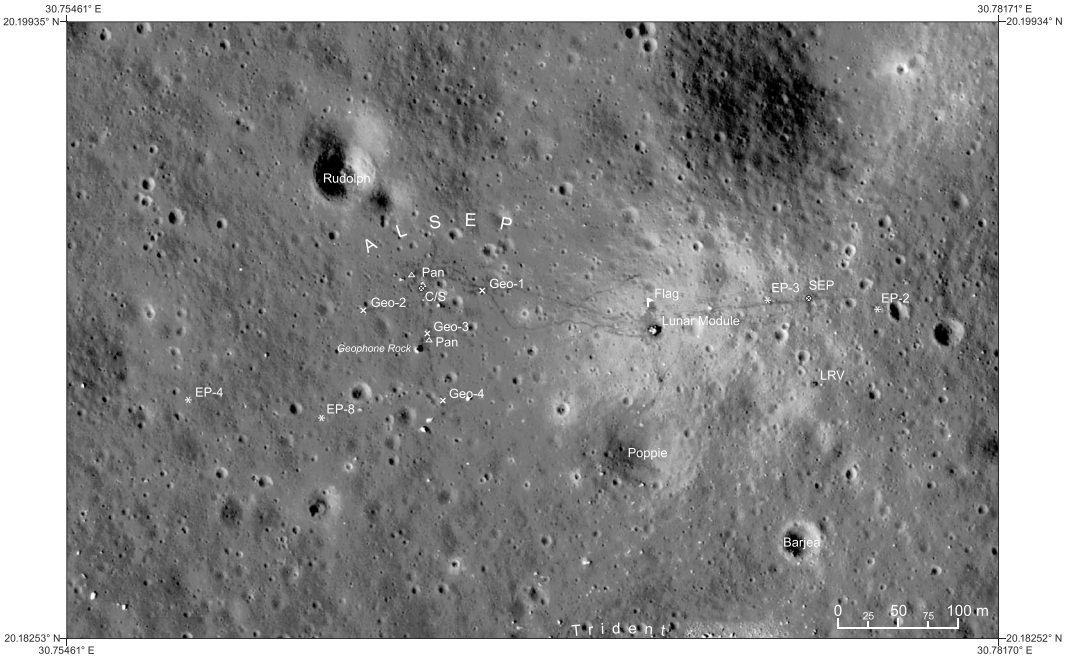


**Figure 26.** Orthomap of the Lunar Module (LM) and Apollo Lunar Surface Experiment Package (ALSEP) region (*Station 0*). The map shows the footprints of the Apollo 17 astronauts and the equipment they installed close to the LM, for example, the array of geophones and the four Explosive Packages deployed nearest to them. The image base is Lunar Reconnaissance Orbiter Camera (LROC) Narrow Angle Camera (NAC) image M168000580R (0.25 m/pixel).

to the LROC orthomosaic using ArcGIS. In parts, the rover was tracked through VLBI observations, which enabled path reconstruction (Salzberg, 1973). In the historic map these sections were drawn in solid lines, whereas the dashed lines represent approximate tracks. We adopted this differentiation and only slightly corrected the course of the traverse at the sites, where the crew had deployed EPs from the rover.

Based on the mapped traverses, we derived profile plots and determined distances traveled, as presented earlier in section 3.2. The total distance traveled during all three EVAs was 31.204 km, and the farthest point traveled from the LM was 7.402 km (linear distance to Station 2). The average speed driven by astronaut Cernan was 6 km/hr (average of all traverses, neglecting short stops). The highest elevation reached by the astronauts by means of the LRV was −2,434.3 m (EVA 2) and the lowest was −2,667.5 m (EVA 3), which corresponds to a height range of 233.2 m in total.

## 4. Discussion

Thirty-seven years past the last manned landing on the Moon the LROC NAC images provide the means for a reinvigorated view of the surface activities of the crew by revealing the traces they have left on the lunar surface. Private initiatives such as the ALSJ or Apollo17.org (Feist et al., 2018) created remarkable online repositories and compilations of Apollo mission data, demonstrating the high value of simultaneous viewing and access to the available resources to get *the big picture*. Likewise, the planetary science community would highly benefit from a Planetary Spatial Data Infrastructure (PSDI), as proposed by the NASA Mapping and Spatial Infrastructure Team (MAPSIT; Lawrence et al., 2016). The goal of the PSDI initiative is to make planetary data easily discoverable, accessible, and usable. While private websites typically aim at providing information according to the timeline of events, a spatial data infrastructure organizes and links data according to location. By relating in situ as well as remote sensing data of multiple instruments and missions, the available data are placed in a broader context and can be fully exploited. The foundation and prerequisite for spatial data analysis are planetary cartographic products as well as geodetically controlled related data. Our cartographic study provides foundational as well as ancillary spatial data of the Apollo 17 landing site.

We generated a controlled DTM of the Taurus-Littrow Valley with a raster grid of 1.5 m and a controlled orthomosaic at 0.5 m/pixel scale. These high-resolution cartographic products allowed registration of

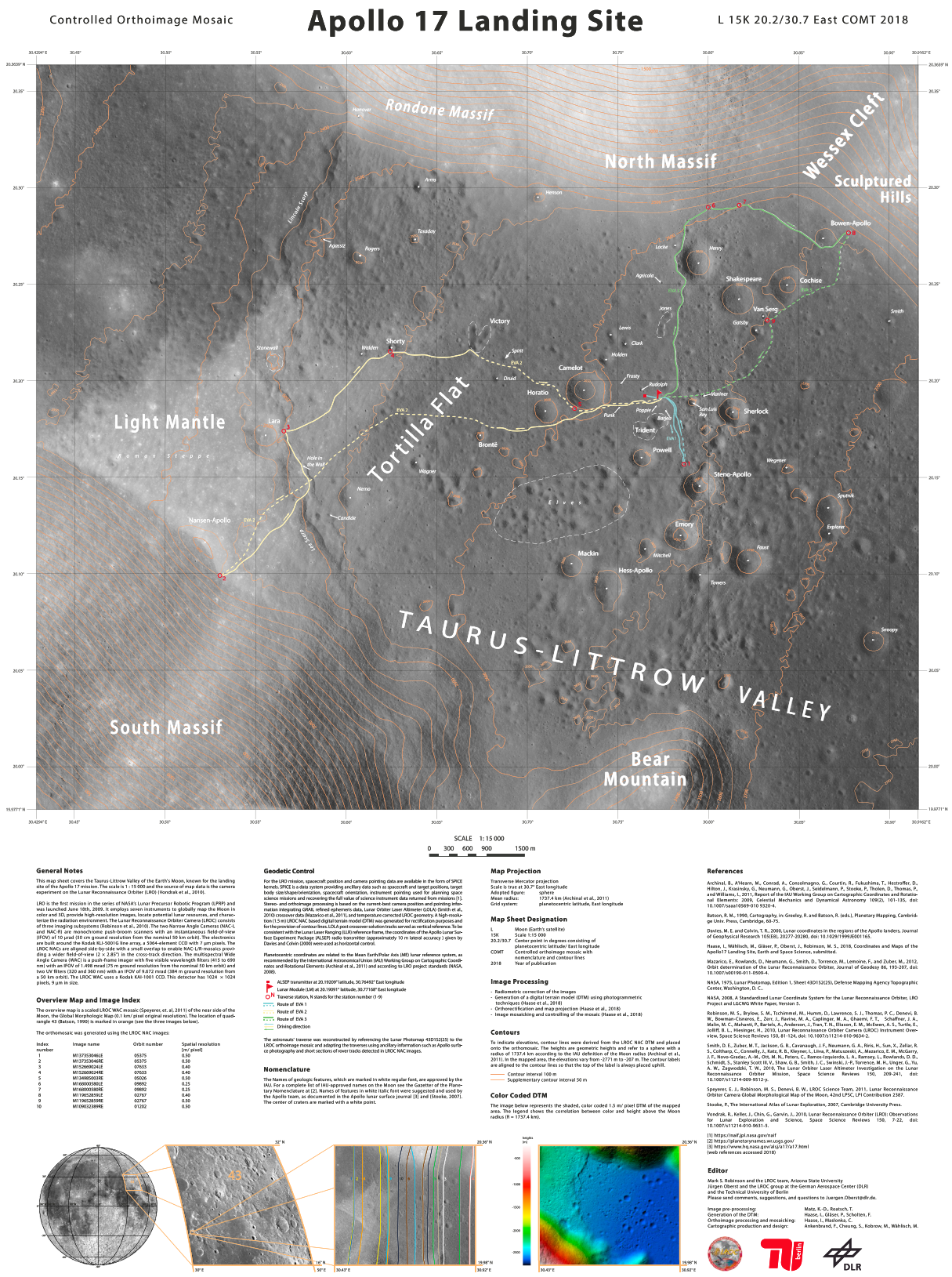


**General Notes**

This map sheet covers the Taurus-Littrow Valley of the Earth's Moon, known for the landing site of the Apollo 17 mission. The scale is 1 : 15 000 and the source of map data is the camera experiment on the Lunar Reconnaissance Orbiter (LRO) (Vondrak et al., 2010).

LRO is the first mission in the series of NASA's Lunar Precursor Robotic Program (LPRP) and was launched June 18th, 2009. It employs seven instruments to globally map the Moon in color and 3D, provide high-resolution images, locate potential lunar resources, and characterize the radiation environment. The Lunar Reconnaissance Orbiter Camera (LROC) consists of three imaging subsystems (Robinson et al., 2010). The two Narrow Angle Cameras (NAC-L and NAC-R) are monochrome push-broom scanners with an instantaneous field-of-view (IFOV) of 10 µrad (50 cm ground resolution from the nominal 50 km orbit). The electronics are built around the Kodak KLI-5001G line array, a 5064-element CCD with 7 µm pixels. The LROC NACs are aligned side-by-side with a small overlap to enable NAC-L/R-mosaics providing a wider field-of-view (2 × 2.85°) in the cross-track direction. The multispectral Wide Angle Camera (WAC) is a push-frame imager with five visible wavelength filters (415 to 690 nm) with an IFOV of 1.498 mrad (75 m ground resolution from the nominal 50 km orbit) and two UV filters (320 and 360 nm) with an IFOV of 9.672 mrad (384 m ground resolution from a 50 km orbit). The LROC WAC uses a Kodak KAI-1001 CCD. This detector has 1024 × 1024 pixels, 9 µm in size.

**Overview Map and Image Index**

The overview map is a scaled LROC WAC mosaic (Speyerer, et. al, 2011) of the near side of the Moon, the Global Morphologic Map (0.1 km/ pixel original resolution). The location of quadrangle 43 (Batson, 1990) is marked in orange (see the three images below).

The orthomosaic was generated using the LROC NAC images:

| Index number | Image name | Orbit number | Spatial resolution [m/ pixel] |
|---|---|---|---|
| 1 | M137353046LE | 05375 | 0.50 |
| 2 | M137353046RE | 05375 | 0.50 |
| 3 | M152909024LE | 07633 | 0.40 |
| 4 | M152909024RE | 07633 | 0.40 |
| 5 | M134985503RE | 05026 | 0.50 |
| 6 | M168000580LE | 09892 | 0.25 |
| 7 | M168000580RE | 09892 | 0.25 |
| 8 | M119652859LE | 02767 | 0.49 |
| 9 | M119652859RE | 02767 | 0.50 |
| 10 | M109032389RE | 01202 | 0.50 |

**Geodetic Control**

For the LRO mission, spacecraft position and camera pointing data are available in the form of SPICE kernels. SPICE is a data system providing ancillary data such as spacecraft and target positions, target body size/shape/orientation, spacecraft orientation, instrument pointing used for planning space science missions and recovering the full value of science instrument data returned from missions [1].

Stereo- and orthoimage processing is based on the current-best camera position and pointing information integrating GRAIL refined ephemeris data, Lunar Orbiter Laser Altimeter (LOLA) (Smith et al., 2010) crossover data (Mazarico et al., 2011), and temperature corrected LROC geometry. A high-resolution (1.5 m) LROC NAC based digital terrain model (DTM) was generated for rectification purposes and for the provision of contour lines. LOLA post crossover solution tracks served as vertical reference. To be consistent with the Lunar Laser Ranging (LLR) reference frame, the coordinates of the Apollo Lunar Surface Experiment Package (ALSEP) radio transmitter (approximately 10 m lateral accuracy ) given by Davies and Colvin (2000) were used as horizontal control.

Planetocentric coordinates are related to the Mean Earth/Polar Axis (ME) lunar reference system, as recommended by the International Astronomical Union (IAU) Working Group on Cartographic Coordinates and Rotational Elements (Archinal et al., 2011) and according to LRO project standards (NASA, 2008).

ALSEP transmitter at 20.19099° latitude, 30.76492° East longitude
Lunar Module (LM) at 20.19093° latitude, 30.77160° East longitude
Traverse station, N stands for the station number (1-9)
Route of EVA 1
Route of EVA 2
Route of EVA 3
Driving direction

The astronauts' traverse was reconstructed by referencing the Lunar Photomap 43D1S2(25) to the LROC orthoimage mosaic and adapting the traverses using ancillary information such as Apollo surface photography and short sections of rover tracks detected in LROC NAC images.

**Nomenclature**

The Names of geologic features, which are marked in white regular font, are approved by the IAU. For a complete list of IAU-approved names on the Moon see the Gazetter of the Planetary Nomenclature at [2]. Names of features in white italic font were suggested and used by the Apollo team, as documented in the Apollo lunar surface journal [3] and (Stooke, 2007). The center of craters are marked with a white point.

**Map Projection**

Transverse Mercator projection
Scale is true at 30.7° East longitude
Adopted figure: sphere
Mean radius: 1737.4 km (Archinal et al., 2011)
Grid system: planetocentric latitude, East longitude

**Map Sheet Designation**

| | |
|---|---|
| L | Moon (Earth's satellite) |
| 15K | Scale 1:15 000 |
| 20.2/30.7 | Center point in degrees consisting of planetocentric latitude/ East longitude |
| COMT | Controlled orthoimage mosaic with nomenclature and contour lines |
| 2018 | Year of publication |

**Image Processing**

- Radiometric correction of the images
- Generation of a digital terrain model (DTM) using photogrammetric techniques (Haase et al., 2018)
- Orthorectification and map projection (Haase et al., 2018)
- Image mosaicking and controlling of the mosaic (Haase et al., 2018)

**Contours**

To indicate elevations, contour lines were derived from the LROC NAC DTM and placed onto the orthomosaic. The heights are geometric heights and refer to a sphere with a radius of 1737.4 km according to the IAU definition of the Moon radius (Archinal et al., 2011). In the mapped area, the elevations vary from -2771 m to -207 m. The contour labels are aligned to the contour lines so that the top of the label is always placed uphill.

Contour interval 100 m
Supplementary contour interval 50 m

**Color Coded DTM**

The image below represents the shaded, color coded 1.5 m/ pixel DTM of the mapped area. The legend shows the correlation between color and height above the Moon radius (R = 1737.4 km).



**References**

Archinal, B., A'Hearn, M., Conrad, A., Consolmagno, G., Courtin, R., Fukushima, T., Hestroffer, D., Hilton, J., Krasinsky, G., Neumann, G., Oberst, J., Seidelmann, P., Stooke, P., Tholen, D., Thomas, P., and Williams, I., 2011, Report of the IAU Working Group on Cartographic Coordinates and Rotational Elements: 2009, Celestial Mechanics and Dynamical Astronomy 109(2), 101–135, doi: 10.1007/saaa10569-010 9320-4.

Batson, R. M., 1990, Cartography, in: Greeley, R. and Batson, R. (eds.), Planetary Mapping, Cambridge Univ. Press, Cambridge, 60-75.

Davies, M. E. and Colvin, T. R., 2000, Lunar coordinates in the regions of the Apollo landers, Journal of Geophysical Research 105(E8), 20277-20280, doi: 10.1029/1999JE001165.

Haase, I., Wählisch, M., Gläser, P., Oberst, J., Robinson, M. S., 2018, Coordinates and Maps of the Apollo 17 Landing Site, Earth and Space Science, submitted.

Mazarico, E., Rowlands, D., Neumann, G., Smith, D., Torrence, M., Lemoine, F., and Zuber, M., 2012, Orbit determination of the Lunar Reconnaissance Orbiter, Journal of Geodesy 86, 193-207, doi: 10.1007/s00190-011-0509-4.

NASA, 1975, Lunar Photomap, Edition 1, Sheet 43D1S2(25), Defense Mapping Agency Topographic Center, Washington, D. C..

NASA, 2008, A Standardized Lunar Coordinate System for the Lunar Reconnaissance Orbiter, LRO Project and LGCWG White Paper, Version 5.

Robinson, M. S., Brylow, S. M., Tschimmel, M., Humm, D., Lawrence, S. J., Thomas, P. C., Denevi, B. W., Bowman-Cisneros, E., Zerr, J., Ravine, M. A., Caplinger, M. A., Ghaemi, F. T., Schaffner, J. A., Malin, M. C., Mahanti, P., Bartels, A., Anderson, J., Tran, T. N., Eliason, E. M., McEwen, A. S., Turtle, E., Jolliff, B. L., Hiesinger, H., 2010, Lunar Reconnaissance Orbiter Camera (LROC) Instrument Overview, Space Science Reviews 150, 81-124, doi: 10.1007/s11214-010-9634-2.

Smith, D. E., Zuber, M. T., Jackson, G. B., Cavanaugh, J. F., Neumann, G. A., Riris, H., Sun, X., Zellar, R. S., Coltharp, C., Connelly, J., Katz, R. B., Kleyner, I., Liiva, P., Matuszeski, A., Mazarico, E. M., McGarry, J. F., Novo-Gradac, A.-M., Ott, M. N., Peters, C., Ramos-Izquierdo, L. A., Ramsey, L., Rowlands, D. D., Schmidt, S., Stanley Scott III, V., Shaw, G. B., Smith, J. C., Swinski, J.-P., Torrence, M. H., Unger, G., Yu, A. W., Zagwodzki, T. W., 2010, The Lunar Orbiter Laser Altimeter Investigation on the Lunar Reconnaissance Orbiter Mission, Space Science Reviews 150, 209-241, doi: 10.1007/s11214-009-9512-y.

Speyerer, E. J., Robinson, M. S., Denevi, B. W., LROC Science Team, 2011, Lunar Reconnaissance Orbiter Camera Global Morphological Map of the Moon, 42nd LPSC, LPI Contribution 2387.

Stooke, P., The International Atlas of Lunar Exploration, 2007, Cambridge University Press.

Vondrak, R., Keller, J., Chin, G., Garvin, J., 2010, Lunar Reconnaissance Orbiter (LRO): Observations for Lunar Exploration and Science, Space Science Reviews 150, 7-22, doi: 10.1007/s11214-010-9631-5.

[1] https://naif.jpl.nasa.gov/naif
[2] https://planetarynames.wr.usgs.gov/
[3] https://www.hq.nasa.gov/alsj/a17/a17.html
(web references accessed 2018)

**Editor**

Mark S. Robinson and the LROC team, Arizona State University
Jürgen Oberst and the LROC group at the German Aerospace Center (DLR)
and the Technical University of Berlin
Please send comments, suggestions, and questions to Juergen.Oberst@dlr.de.

| | |
|---|---|
| Image pre-processing: | Matz, K.-D., Roatsch, T. |
| Generation of the DTM: | Haase, I., Gläser, P., Scholten, F. |
| Orthoimage processing and mosaicking: | Haase, I., Wählisch, C. |
| Cartographic production and design: | Ankenbrand, F., Cheung, S., Kobrow, M., Wählisch, M. |



**Figure 27.** Lunar Reconnaissance Orbiter Camera (LROC) Narrow Angle Camera (NAC) based controlled orthoimage map of the Apollo 17 Landing Site.

Hasselblad photographs and to provide absolute camera positions to 1-m scale accuracy (and better in some cases). From these newly controlled astronaut images, accurate estimates of the size and location of landforms and hardware are derived enhancing our ability to provide context to a host of derived measurements. Image (re) analysis benefits from the recent scans of the original Hasselblad flight film providing new research possibilities through digital image processing techniques. For example, by applying close range photogrammetry to the controlled Hasselblad images and by reconstructing extensive 3-D scenes as presented by Schmitt et al. (2017) regional surface models of very high resolution can be integrated and jointly analyzed with the LROC NAC based DTM and orthomap. Relative measurements obtained from Hasselblad images tied to the higher level ME-coordinate system allow automatic correlation to features seen in the LROC NAC orthoimages.

Furthermore, the acquisition and mapping of the geolocations of the ALSEP instruments at half meter scale accuracy enable a new look at the original measurements acquired by ALSEP experiments. For example, by determining the EP positions with accuracies of 0.5 to 3.0 m we were able to provide improved source-receiver distances of the active seismic experiment LSPE. Distances along with times are essential in the analysis of seismic recordings. First results of Heffels et al. (2017), who integrated our improved distances into their computations, lead to new velocity-depth profiles of the Apollo 17 site and refined two- and three-layer seismic velocity models of the upper crust.

Concerning future missions, the most accurate and detailed knowledge of the regional topography is crucial in landing site selection, a safe landing, and efficient mission operations. Topographic surface models and maps as provided by this study support mission planning and are used to assist rover navigation and determine least work traverses. Furthermore, in the case of former landing sites, precise knowledge of the geolocations of mission relics contributes to the protection of human heritage sites during future landings, as planned, for example, by the *PTScientists*.

## 5. Summary and Conclusion

From high-resolution LROC NAC stereo images we derived a controlled DTM and orthomosaic of the Apollo 17 landing site area. The orthomosaic provided control information to register close-range surface images to the orbital images by applying a least squares (2-D) network adjustment. By doing so we provided a cartographic context to the historic astronaut photographs. Based on that, geolocations of all of the ALSEP instruments and mission equipment were determined by triangulation. We mapped the determined geolocations in the controlled LROC NAC orthomosaic and created a new Apollo 17 Landing Site Map (scale 1:15000). In addition, we provide large-scale maps (1:1000) of the individual traverse stations and the ALSEP site, profiles of the EVA traverses, and improved LSPE source-receiver distances. Furthermore, a list of newly measured crater diameters and positions are provided supplementary to this study.

High-level planetary data products, that is, geodetically controlled DTMs and orthomosaics, are the required foundation for spatial data driven research. Controlled maps and ancillary geospatial data of the Apollo 17 landing site are equally important in the improved reanalysis of the invaluable on-site experiments, in the planning and operation of future missions, but also in the preservation and protection of the achievements of human space flight. In addition, the registration approach presented here, which links close-range surface images with data from orbital images, can be used for astronaut or rover localization. While the current implementation of the method requires significant manual interaction, further studies on automatic image correlation can be of considerable value.

## 6. Outlook

We are currently investigating the feasibility of applying a photogrammetric (3-D) space resection to determine the camera's attitude angles in addition to its absolute position, that is, going from 2-D to 3-D by solving for the full six parameters of a camera's Exterior Orientation ($X,Y,Z,\omega,\varphi,\kappa$). To obtain a unique and stable solution, the control points picked from the surface and the orbital images are required to be well distributed over the image frame.

We also plan to further exploit the Hasselblad images to determine individual locations from where the astronauts collected rock samples and obtained drill cores. The results will be mapped in the large-scale station maps and may also be integrated into a spatial data infrastructure to support integrated and multisource scientific analyses.

To further improve the relative and absolute accuracy of the LROC NAC DTMs, we are currently implementing a bundle adjustment incorporating LOLA and LLR ground control. By exploiting the geometric identities of stereo imagery and tying the object model to coregistered LOLA shots, errors in the exterior orientation of the LROC NACs are minimized aiming for exact forward ray intersections.

## Appendix A

See Tables A1–A5.

**Table A1**
*Image Parameters of the LROC NAC Stereo Pairs*

| LROC NAC | Orbit | Resolution (m/pixel) | Incidence angle (°) | Slew angle (°) | Included in... |
|---|---|---|---|---|---|
| M137346262-L/-R | 5374 | 0.5 | 41 | −18 | DTM |
| M137353046-L/-R | 5375 | 0.5 | 41 | +17 | DTM/ortho |
| M159746082-L/-R | 8676 | 0.5 | 50 | +21 | DTM |
| M159752868-L/R | 8677 | 0.5 | 49 | −18 | DTM |
| M190394800-R | 13104 | 1.0 | 46 | +4 | DTM |
| M190401948-L | 13105 | 1.0 | 45 | −4 | DTM |
| M134985003-L/-R | 5026 | 0.5 | 64 | −20 | DTM/ortho |
| M134991788-L/-R | 5027 | 0.5 | 65 | +15 | DTM |
| M152669024-L/-R | 7633 | 0.4 | 39 | +24 | DTM/ortho |
| M152675807-L/-R | 7634 | 0.5 | 40 | −14 | DTM |

*Note.* Five stereo image pairs were used to process the LROC NAC DTM (1.5 m/pixel) of the Apollo 17 landing site (sorted from west to east). The last column provides information on whether individual stereo images were also included in the orthomosaic. DTM, digital terrain model; LROC, Lunar Reconnaissance Orbiter Camera; NAC, Narrow Angle Camera.

**Table A2**
*NAIF SPICE Kernels Used to Determine LROC NAC Position and Pointing*

| Description | Data file |
|---|---|
| Planetary and lunar ephemeris | de421.bsp |
| planetary constants | moon_pa_de421_1900–2050.bpc |
| planetary and lunar orientation/size/shape | pck00010.tpc |
| lunar frames | moon_080317.tf |
| | moon_assoc_me.tf |
| LRO ephemeris | lro_*_grgm900c_l600.bsp |
| LRO frame definitions | lro_frames_2014049_v01.tf |
| LRO/LROC orientation | moc42_*.bc |
| | soc31_*.bc |
| LRO clock correction | lro_clkcor_2014197_v00.tsc |
| leap-seconds | naif0010.tls |

*Note.* LROC, Lunar Reconnaissance Orbiter Camera; NAC, Narrow Angle Camera; NAIF, Navigation and Ancillary Information Facility.

**Table A3**
*LROC NAC Images Used to Create the Apollo 17 Orthomosaic (0.5 m/pixel)*

| LROC NAC image | Orbit | Resolution (m/pixel) | Incidence angle (°) | Slew angle (°) | Sun direction |
|---|---|---|---|---|---|
| M137353046-L/-R | 5375 | 0.5 | 41 | +17 | w |
| M152669024-L/-R | 7633 | 0.4 | 39 | +24 | w |
| M134985003-R | 5026 | 0.5 | 64 | −20 | w |
| M168000580-L/-R | 9892 | 0.3 | 45 | −26 | w |
| M119652859-L/-R | 2767 | 0.4/0.5 | 59 | −20 | w |
| M109032389-R | 1202 | 0.5 | 22 | −20 | w |

*Note.* The images are listed in the order of layering from the top to the bottom layer of the mosaic. LROC, Lunar Reconnaissance Orbiter Camera; NAC, Narrow Angle Camera.

**Table A4**
*List of Acronyms*

| Acronym | Instrument | Acronym/abbreviation | Instrument |
|---|---|---|---|
| C/S | Central Station | LSP | Lunar seismic profiling |
| RTG | Radioisotope Thermoelectric Generator | G/M | Geophone module |
| HFE | Heat Flow Experiment | Geo-1 | Geophone number 1 |
| LACE | Lunar Atmosphere Composition Experiment | SEP | Surface Electrical Properties |
| LEAM | Lunar Ejecta and Meteorites | LM | Lunar Module |
| LSG | Lunar Surface Gravimeter | LRV | Lunar Roving Vehicle |

**Table A5**
*Distances Between the Seismic Sources and the Individual Geophones*

| Source | Geophone | Distance (m) | Cooper and Kovach (m) | Difference (m) |
|---|---|---|---|---|
| EP-8 | 1 | 169.4 | 179 | −9.6 |
| | 2 | 95.0 | 101 | −6.0 |
| | 3 | 111.9 | 122 | −10.1 |
| | 4 | 101.4 | 112 | −10.6 |
| LM ascent | 1 | 145.6 | 148[a] | −2.4 |
| | 2 | 240.9 | 244[a] | −3.1 |
| | 3 | 187.1 | 190[a] | −2.9 |
| | 4 | 183.3 | 187[a] | −3.7 |
| EP-4 | 1 | 259.5 | 269 | −9.5 |
| | 2 | 162.4 | 172 | −9.6 |
| | 3 | 205.4 | 215 | −9.6 |
| | 4 | 210.9 | 220 | −9.1 |
| EP-3 | 1 | 236.3 | 242 | −5.7 |
| | 2 | 334.9 | 341 | −6.1 |
| | 3 | 282.9 | 288 | −5.1 |
| | 4 | 281.0 | 287 | −6.0 |
| EP-2 | 1 | 327.4 | 327 | 0.4 |
| | 2 | 425.6 | 425 | 0.6 |
| | 3 | 372.9 | 371 | 1.9 |
| | 4 | 367.2 | 366 | 1.2 |
| EP-7 | 1 | 785.1 | 800 | −14.9 |
| | 2 | 840.8 | 865 | −24.2 |
| | 3 | 789.8 | 810 | −20.2 |
| | 4 | 741.7 | 672[b] (762) | 69.7 (−20.3) |
| EP-6 | 1 | 1,200.7 | 1,195 | 5.7 |
| | 2 | 1,236.1 | 1,240 | −3.9 |
| | 3 | 1,192.3 | 1,195 | −2.7 |
| | 4 | 1,138.2 | 1,095 | 43.2 |
| EP-5 | 1 | 2,225.9 | 2,230 | −4.1 |
| | 2 | 2,318.4 | 2,330 | −11.6 |
| | 3 | 2,283.2 | 2,290 | −6.8 |
| | 4 | 2,302.6 | 2,320 | −17.4 |
| EP-1 | 1 | 2,892.4 | 2,855 | 37.4 |
| | 2 | 2,801.5 | 2,758 | 43.5 |
| | 3 | 2,857.7 | 2,818 | 39.7 |
| | 4 | 2,885.5 | 2,870 | 15.5 |

*Note*. The distances used for modeling the near-surface lunar structure at Apollo times (Cooper & Kovach, 1975) are included for comparison. The seismic sources are listed in increasing order of distance to the array of geophones. [a]Distances published by (Kovach et al., 1973). [b]Most probable a transposition of numbers in the table given by Cooper and Kovach (1975). Here a distance of 762 m is more plausible (corrected values are given in brackets).

**Acknowledgments**
This work was supported by the German Federal Ministry for Economic Affairs and Energy (FKZ 50OW1702). We acknowledge the NASA LRO Missions Operations Team at Goddard Space Flight Center and thank the LROC Science Operations Team at Arizona State University for constant expert support and amicable collaboration. Special thanks go to Shu Kwaun Cheung, Fabian Ankenbrandt, Miriam Kobrow, and Cindy Maslonka of the Beuth University of Applied Sciences for their cartographic expertise and support. We would like to thank Ken Edmundson and the anonymous reviewer for their valuable comments. Newly measured locations and diameters of the Apollo 17 craters are provided as supporting information to this article. The LROC NAC DTM, the orthomosaic, the digitized traverse, and the Apollo 17 Landing Site Map (in print resolution) are archived in the PDS Cartography and Imaging Sciences Node (IMG) Annex and can be accessed at https://astrogeology.usgs.gov/pds/annex.

## References

Acton, C. H. (1996). Ancillary data services of NASA's navigation and ancillary information facility. *Planetary and Space Science*, *44*, 65–70. https://doi.org/10.1016/0032-0633(95)00107-7

Apollo 17 Mission Evaluation Team (1973). Apollo 17 mission report. National Aeronautics and Space Administration (NASA), Johnson Space Center, document JSC-07904.

Borgeson, W. T., & Batson, R. M. (1969). Photogrammetric calibration of Apollo film cameras. USGS Open-File Report, N69–N27911.

Cooper, M. R., & Kovach, R. L. (1975). Energy, frequency, and distance of moonquakes at the Apollo 17 site. Proceedings of the Conference Paper presented at the 6th Lunar and Planetary Science, 2863–2879.
Costes, N. C., Farmer, J. E., & George, E. B. (1972). Mobility performance of the lunar roving vehicle: Terrestrial studies: Apollo 15 results. NASA Technical Report, NASA-TR-R-401.
Davies, M. E., & Colvin, T. R. (2000). Lunar coordinates in the regions of the Apollo landers. *Journal of Geophysical Research*, *105*(E8), 20,277–20,280. https://doi.org/10.1029/1999JE001165
Defense Mapping Agency (1975). Apollo 17 Traverses Lunar Photomap 1:25000. Defense Mapping Agency Topographic Center, Washington, D. C., Edition 1, Sheet 43D1S2(25).
Feist, B., Bleacher, J. E., Petro, N. E., & Niles, P. B. (2018). Documenting of geologic field activities in real time in four dimensions: Apollo 17 as a case study for terrestrial analogues and future exploration. In 49th Lunar and Planetary Science Conference, Texas (P. 2681).
Garrett, D. (1972). Apollo 17 press kit. National Aeronautics and Space Administration (NASA), Washington, D. C., release no. 72-220K.
Gläser, P., Haase, I., Oberst, J., & Newmann, G. A. (2013). Co-registration of laser altimeter tracks with digital terrain models and applications in planetary science. *Planetary and Space Science*, *89*, 111–117. https://doi.org/10.1016/j.pss.2013.09.012
Haase, I., Oberst, J., Scholten, F., Wählisch, M., Gläser, P., Karachevtseva, I., & Robinson, M. S. (2012). Mapping the Apollo 17 landing site area based on Lunar Reconnaissance Orbiter Camera images and Apollo surface photography. *Journal of Geophysical Research*, *117*, E00H20. https://doi.org/10.1029/2011JE003908
Haruyama, J., Ohtake, M., Matsunaga, T., Otake, H, Ishihara, Y., Masuda, K., et al. (2014). Data products of Selene (Kaguya) terrain camera for future lunar missions. In 45th Lunar and Planetary Science Conference, Texas (P. 1304).
Heffels, A., Knapmeyer, M., Oberst, J., & Haase, I. (2017). Re-evaluation of Apollo 17 lunar seismic profiling experiment data. *Planetary and Space Science*, *135*, 43–54. https://doi.org/10.1016/j.pss.2016.11.007
Kammerer, J., & Zeiss, C. (1972). The moon camera and its lenses. *Optical Engineering*, *11*(2), 73–78. https://doi.org/10.1117/12.7971614
Karachevtseva, I., Oberst, J., Scholten, F., Konopikhin, A., Shingareva, K., Cherepanova, E., et al. (2013). Cartography of the Lunokhod-1 landing site and traverse from LRO image and stereo-topographic data. *Planetary and Space Science*, *85*, 175–187. https://doi.org/10.1016/j.pss.2013.06.002
Karachevtseva, I. P., Kozlova, N. A., Kokhanov, A. A., Zubarev, A. E., Nadezhdina, I. E., Patratiy, V. D., et al. (2017). Cartography of the Luna-21 landing site and Lunokhod-2 traverse area based on Lunar Reconnaissance Orbiter Camera images and surface archive TV-panoramas. *Icarus*, *283*, 104–121. https://doi.org/10.1016/j.icarus.2016.05.021
Keller, J. W., Petro, N. E., Vondrak, R. R., & the LRO team (2016). The Lunar Reconnaissance Orbiter mission—Six years of science and exploration at the Moon. *Icarus*, *273*, 2–24. https://doi.org/10.1016/j.icarus.2015.11.024
King, R. W., Counselmann, C. C., & Shapiro, I. I. (1976). Lunar dynamics and selenodesy: Results from analysis of VLBI and laser data. *Journal of Geophysical Research*, *81*(35), 6251–6256. https://doi.org/10.1029/JB081i035p06251
Kovach, R. L., Watkins, J. S., & Talwani, P. (1973). Lunar Seismic Profiling Experiment. In Apollo 17 Preliminary Science Report, NASA SP-330, 10.1–10.12.
Lauderdale, W. W., & Eichelman, W. F. (1974). Apollo scientific experiments data handbook. National Aeronautics and Space Administration (NASA), Johnson Space Center, Technical Memorandum, NASA TM X-58131, document JSC-09166.
Lawrence, S. J., Hagerty, J., Gaddis, L. R., Archinal, B. A., Radebaugh, J., Byrne, S., et al. (2016). The Mapping and Planetary Spatial Infrastructure Team (MAPSIT): Addressing strategic planning needs for planetary cartography. In 47th Lunar and Planetary Science Conference, Texas (P. 1710).
Lawrence, S. J., Robinson, M. S., Broxton, M., Stopar, J. D., Close, W., Grunsfeld, J., et al. (2008). The Apollo digital image archive: New research and data products. In Proceedings of the NLSI Lunar Science Conference, (P. 2066).
Lemoine, F. G., Goossens, S., Sabaka, T. J., Nicholas, J. B., Mazarico, E., Rowlands, D. D., et al. (2014). GRGM900C: A degree 900 lunar gravity model from GRAIL primary and extended mission data. *Geophysical Research Letters*, *41*, 3382–3389. https://doi.org/10.1002/2014GL060027
Malhotra, R. C. (1972). Calibration of Apollo 16 lunar surface 60 mm Hasselblad cameras on Wild T-4 goniometer. NASA Technical Report, LEC/HASD no. 640-TR-055.
Mazarico, E., Lemoine, F. G., Goossens, S. J., Sabaka, T. J., Nicholas, J. B., Rowlands, D. D., et al. (2013). Improved precision orbit determination of lunar orbiters from the GRAIL-derived gravity models. In Proceedings of the 23rd AAS/AIAA Space Flight Mechanics Conference, Kauai, Hawai, AAS 13–274.
Mazarico, E., Rowlands, D. D., Neumann, G. A., Smith, D. E., Torrence, M. H., Lemoine, F. G., & Zuber, M. T. (2012). Orbit determination of the Lunar Reconnaissance Orbiter. *Journal of Geodesy*, *86*(3), 193–207. https://doi.org/10.1007/s00190-011-0509-4
Mühlberger, W. R., Batson, R. M., Cernan, E. A., Freeman, V. L., Hait, M. H., Holt, H. E., et al. (1973). Preliminary geologic investigation of the Apollo 17 landing site. In Apollo 17 Preliminary Science Report, NASA SP-330, 6.1–6.91.
National Aeronautics and Space Administration (2018). Retrieved from https://www-mipl.jpl.nasa.gov/external/vicar.html, (last date accessed: 20 February 2018).
Pustynski, V.-V., & Jones, E. M. (2014). Photogrammetry of Apollo 11 surface imagery. *Journal of the British Interplanetary Society*, *67*(10), 390–398.
Robinson, M. S., Brylow, S. M., Tschimmel, M., Humm, D., Lawrence, S. J., Thomas, P. C., et al. (2010). Lunar Reconnaissance Orbiter Camera (LROC) Instrument Overview. *Space Science Reviews*, *150*(1-4), 81–124. https://doi.org/10.1007/s11214-010-9634-2
Salzberg, I. M. (1973). Tracking of the Apollo lunar rover with interferometry techniques. *Proceedings of the Institute of Electrical and Electronics Engineers*, *61*(9), 1233–1236. https://doi.org/10.1109/PROC.1973.9251
Schmitt, H. H., Petro, N. E., Wells, R. A., Robinson, M. S., Weiss, B. P., & Mercer, C. M. (2017). Revisiting the field geology of Taurus–Littrow. *Icarus*, *298*, 2–33. https://doi.org/10.1016/j.icarus.2016.11.042
Scholten, F., Gwinner, K., Roatsch, T., Matz, K. D., Wählisch, M., Giese, B., Oberst, J., et al. (2005). Mars express HRSC data processing—Methods and operational aspects. *Photogrammetric Engineering & Remote Sensing*, *71*(10), 1143–1152. https://doi.org/10.14358/PERS.71.10.1143
Scholten, F., Oberst, J., Matz, K.-D., Roatsch, T., Wählisch, M., Speyerer, E. J., & Robinson, M. S. (2012). GLD100: The near-global lunar 100 m raster DTM from LROC WAC stereo image data. *Journal of Geophysical Research*, *117*, E00H17. https://doi.org/10.1029/2011JE003926
Smith, E. C., & Mastin, W. C. (1973). Lunar roving vehicle navigation system performance review. NASA Technical Report, NASA-TN-D-7469.
Sollberger, D., Schmelzbach, C., Robertsson, J. O. A., Greenhalgh, S. A., Nakamura, Y., & Khan, A. (2016). The shallow elastic structure of the lunar crust: New insights from seismic wavefield gradient analysis. *Geophysical Research Letters*, *43*, 10,078–10,087. https://doi.org/10.1002/2016gl070883

Speyerer, E. J., Wagner, R. V., Robinson, M. S., Licht, A., Thomas, P. C., Becker, K., et al. (2014). Pre-flight and on-orbit geometric calibration of the Lunar Reconnaissance Orbiter Camera. *Space Science Reviews*, *200*(1-4), 357–392. https://doi.org/10.1007/s11214-014-0073-3

Tanimoto, T., Eitzel, M., & Yano, T. (2008). The noise cross-correlation approach for Apollo 17 LSPE data: Diurnal change in seismic parameters in shallow lunar crust. *Journal of Geophysical Research*, *113*, E08011. https://doi.org/10.1029/2007JE003016

Wagner, R. V., Nelson, D. M., Plescia, J. B., Robinson, M. S., Speyerer, E. J., & Mazarico, E. (2016). Coordinates of anthropogenic features on the moon. *Icarus*, *283*, 92–103. https://doi.org/10.1016/j.icarus.2016.05.011

Wewel, F. (1996). Determination of conjugate points of stereoscopic three line scanner data of Mars96 Mission. *International Archives of Photogrammetry and Remote Sensing*, *31*(B3), 936–939.

Wolfe, E. W., Bailey, N. G., Lucchitta, B. K., Muehlberger, W. R., Scott, D. H., Sutton, R. L., & Wilshire, H. G. (1981). The geologic investigation of the Taurus-Littrow Valley: Apollo 17 Landing Site, with a section on Apollo 17 lunar surface photography. USGS Report, Professional Paper 1080, 280 p.